*Geophys. J. Int.* (2000) **143,** 52–70

# Convective instability of thickening mantle lithosphere

Clinton P. Conrad*

*Department of Earth, Atmospheric, and Planetary Sciences, Massachusetts Institute of Technology, Cambridge,* MA 02139, *USA*

Accepted 2000 April 17. Received 2000 April 12; in original form 1999 June 28

## SUMMARY

Mantle lithosphere, being colder and therefore denser than the underlying mantle, is prone to convective instability that can be induced by horizontal shortening. Numerical experiments on a cold layer with imposed horizontal shortening are carried out to examine the relative importance of mechanical thickening, thermal diffusion and gravitational instability in deforming the layer. This analysis is then used to develop a method for determining which of these styles dominates for a layer thickening at a given rate. If viscosity is non-Newtonian, the imposition of shortening decreases the lithospheric strength, which causes perturbations to the lithosphere's temperature structure to grow exponentially with time. Once these perturbations become sufficiently large, they then grow super-exponentially with time, eventually removing the lithospheric base. Because lithospheric viscosity is highly temperature-dependent, at most only the lower 30 per cent of the lithosphere participates in the downwelling associated with this initial super-exponential growth event. After this event, however, a downwelling develops that removes material advected into the region of downwelling by horizontal shortening. The magnitude of this persistent downwelling depends on the rate and duration of shortening. If the total amount of shortening does not exceed 50 per cent (doubling of crustal thickness), then this downwelling extends to a depth three to four times the thickness of undeformed lithosphere and forms a sheet significantly thinner than the width of the region undergoing shortening. Once shortening stops, this downwelling is no longer replenished by the shortening process, and should then detach due to its inherent gravitational instability. The hottest 60 per cent of the mantle lithosphere could be removed in such an event, which would be followed by an influx of hot, buoyant asthenosphere that causes rapid surface uplift. Because more cold material is removed after the cessation of shortening than by the initial gravitational instability, the former has a potentially greater influence on surface uplift. The Tibetan interior is thought to have been shortened by about 50 per cent in $\sim$30 Myr and afterwards, at $\sim$8 Ma, experienced a period of rapid uplift that may have resulted from the removal of a large downwelling 'finger' of cold lithosphere generated by shortening.

**Key words:** convective instability, gravitational instability, mantle lithosphere, thermal diffusion, Tibet, viscosity.

## INTRODUCTION

Thickening of the crust is one consequence of horizontal convergence at the Earth's surface and is the main process by which mountains are built. Thickening of mantle lithosphere may occur as well, and has been proposed as an accompanying process that may also affect mountain building. In particular, thickening should enhance the gravitational instability of cold, dense mantle lithosphere with respect to the hot, buoyant asthenosphere beneath it (Fig. 1a) (e.g. Fleitout & Froidevaux 1982; Houseman *et al.* 1981). If the mantle lithosphere becomes sufficiently unstable, localized convective downwelling, of the type described by Howard (1964), may be initiated at the base of the mantle lithosphere (Fig. 1b). The subsequent removal of cold lithosphere, and its replacement by hot mantle, could result in rapid surface uplift followed by extension (e.g. Bird 1979; England & Houseman 1989; Neil & Houseman 1999). This process is thought to have caused rapid uplift of the Tibetan plateau 8 Myr ago (Harrison *et al.* 1992; Molnar *et al.* 1993), and has been inferred for other mountain belts (Houseman & Molnar 1997; Platt & England 1994; Platt *et al.* 1998).

*Now at: Seismological Laboratory, California Institute of Technology, Pasadena, CA 91125, USA. E-mail: clint@gps.caltech.edu

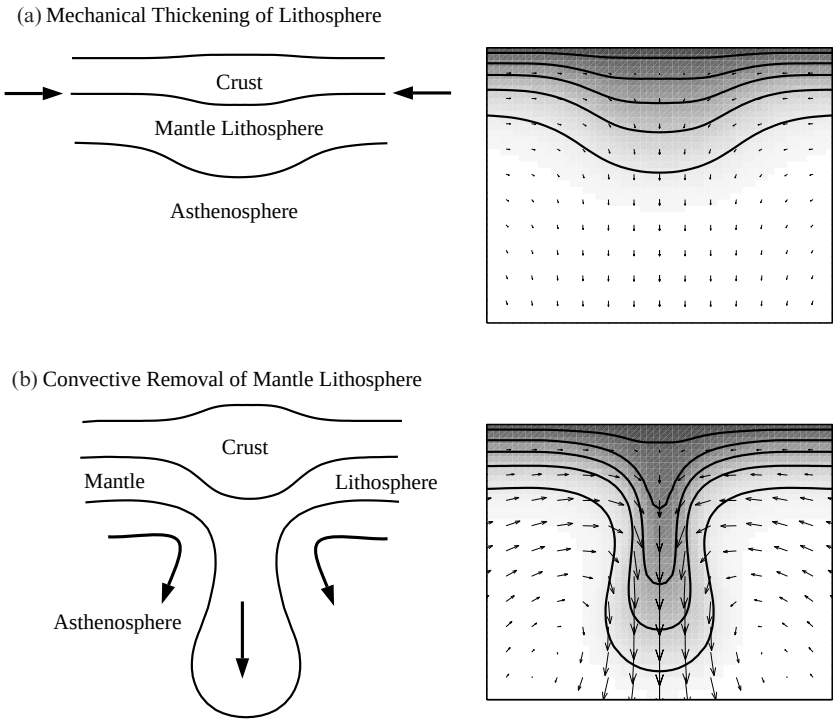


**Figure 1.** Cartoons showing (a) horizontal shortening and thickening of the lithosphere, including its mantle portion. Mechanical thickening should enhance the gravitational instability of the cold, dense, mantle lithosphere with respect to the hot asthenosphere below. If the mantle lithosphere is made sufficiently unstable, its lower portion may be removed in a localized convective downwelling, drawn in (b). Removal of mantle lithosphere and its replacement by hot asthenosphere could result in rapid uplift at the surface. Shown on the right in both (a) and (b) is output from a numerical experiment that shows the generation of convective instability by mechanical thickening of a cold, dense layer. Here arrows represent velocity and show horizontal shortening of the central region in (a) and a faster flow associated with convective downwelling in (b). Temperature, represented by shades of grey (colder is darker) and contours (evenly spaced temperature intervals), clearly shows the removal of the cold layer's basal portion.

The gravitational instability of mantle lithosphere can be enhanced by thickening in several ways. First, thickening increases the amount of dense, potentially unstable material in a thickened region (e.g. Conrad & Molnar 1999; Fleitout & Froidevaux 1982; Houseman *et al.* 1981). Second, if lithospheric rocks deform by a non-linear stress–strain relationship, as they are observed to do in laboratory experiments, the strain rates associated with shortening should decrease the background strength of the lithosphere and enhance its gravitational instability (Molnar *et al.* 1998). Finally, non-uniform thickening generates large variations in the lithosphere's stratified temperature field, allowing gravitational instability to grow from accompanying variations in the density field. If viscosity is non-Newtonian, the strain rates associated with the growing instability decrease the lithosphere's strength and cause the instability to grow more rapidly. This process accelerates into a rapid removal of the lithospheric base (e.g. Canright & Morris 1993; Conrad & Molnar 1999; Houseman & Molnar 1997).

These mechanisms of promoting gravitational instability of the lithosphere have been studied by approximating the convective instability as a Rayleigh–Taylor instability, in which diffusion of heat is ignored. Thermal diffusion, however, smoothes perturbations to the lithosphere's stratified temperature field, and thus may retard, or even prevent, their growth as part of convective instability. Conrad & Molnar (1999) addressed this issue by including the stabilizing effects of thermal diffusion for a generalized density and viscosity structure. These authors, however, studied instability only in layers that were already convectively unstable, and considered horizontal shortening only as a mechanism that allows the lithosphere to thicken into an unstable state. The role of horizontal shortening in making lithosphere unstable was treated more fully by Molnar *et al.* (1998), but their studies did not include thermal diffusion. Thus, an analysis of the full convective instability for a layer that is undergoing horizontal shortening is needed.

The numerical experiments described below, which are similar to those exemplified in Fig. 1, simulate mantle lithosphere that eventually becomes convectively unstable because it thickens. I compare the deformation that results to the unstable growth predicted by simpler studies of the Rayleigh–Taylor instability for different rheologies (e.g. Conrad & Molnar 1997, 1999; Houseman & Molnar 1997), undergoing horizontal shortening (e.g. Molnar *et al.* 1998), and in conjunction with thermal diffusion (e.g. Conrad & Molnar 1999). The rheological conditions and magnitudes of shortening rates that generate the various types of gravitational instability can then be determined in a general way using a dimensionless scaling analysis, as can the approximate time-dependent behaviour of a growing instability. Finally, I attempt to determine how much material may be removed by convective instability in a thickening environment, and the effect of this removal on the remaining lithosphere. As a result, this study treats the full convective instability of thickening mantle lithosphere more completely than do previous analyses. Because they build upon previously developed scaling analyses for various aspects of the full problem treated here, these results are comprehensive, but easily applied to gravitationally unstable layered structures such as the mantle lithosphere.

## REVIEW OF RATES FOR UNSTABLE GROWTH

The convective stability of a thickening cold thermal boundary layer can be studied by observing the behaviour of small perturbations to the boundary layer's stratified temperature field. Various timescales are associated with different mechanisms that promote the growth or decay of these perturbations. The first growth mechanism is the shortening process itself, which advects cold material downwards as the layer thickens, and therefore amplifies perturbations to the temperature field (e.g. Bassi & Bonnin 1988; Fletcher & Hallet 1983; Ricard & Froidevaux 1986; Zuber *et al.* 1986). Two types of growth are associated with the gravitational instability of a dense fluid overlying a less dense fluid, also known as a Rayleigh–Taylor instability. If the viscosity of the deforming fluid is independent of strain rate, perturbations initially grow exponentially with time (e.g. Chandrasekhar 1961; Conrad & Molnar 1997; Whitehead & Luther 1975). For non-Newtonian viscosity, growth is super-exponential with time (e.g. Canright & Morris 1993; Houseman & Molnar 1997). Finally, the lithosphere's density field is perturbed through temperature, which is subject to thermal diffusion. Thermal diffusion smoothes temperature variations and thus diminishes the amplitude of density perturbations, slowing, or even preventing, their unstable growth (e.g. Rayleigh 1916).

The complete convective instability of a thickening boundary layer with non-Newtonian viscosity can thus be ideally described as the simultaneous action of (a) mechanical thickening, (b) exponential followed by (c) super-exponential growth of perturbations, and (d) thermal diffusion acting to suppress growth. Each mechanism operates with a characteristic timescale that depends on the size of the perturbation itself and on the physical properties of the layer. In general, one of the four mechanisms has a dominant influence on the behaviour of perturbations because it induces growth or decay of perturbations at significantly faster rates than do the others. In what follows, expressions for these growth or decay rates are developed. These expressions are later used to construct dimensionless parameters that compare the relative importance of the different mechanisms in deforming a given thermal boundary layer that is undergoing horizontal shortening.

### Exponential growth

If thermal diffusion is ignored, perturbations to an unstable density structure grow in a manner that can be described by an analysis of the Rayleigh–Taylor instability. In this analysis, it is useful to describe deformation of a fluid by a strain rate, $\dot{\varepsilon}_{ij}$, defined in terms of the components of velocity, $u_i$:

$$\dot{\varepsilon}_{ij} = \frac{1}{2}\left(\frac{\partial u_i}{\partial x_j} + \frac{\partial u_j}{\partial x_i}\right). \tag{1}$$

The flow field is incompressible, meaning that $\dot{\varepsilon}_{ii} = 0$. In a highly viscous fluid, gravitational body forces are balanced by viscous stresses associated with flow. This flow, described by the strain rate, is related to the deviatoric stress, $\tau_{ij}$, by

$$\tau_{ij} = 2\eta\dot{\varepsilon}_{ij}\,. \tag{2}$$

The effective viscosity, $\eta$, can vary with temperature and may depend on strain rate,

$$\eta = \frac{B}{2}\,\dot{E}^{\left(\frac{1}{n}-1\right)}, \tag{3}$$

where $B$ is a rheological parameter, $n$ is a power-law exponent and $\dot{E}^2 = (1/2)\sum_{i,j}\dot{\varepsilon}_{ij}\cdot\dot{\varepsilon}_{ij}$ is the second invariant of the strain-rate tensor. Dislocation creep of olivine in the lithosphere is often described using eq. (3) and $n$ about 3.5 (e.g. Kohlstedt *et al.* 1995).

For Newtonian viscosity ($n = 1$), $\eta = B/2$ is a constant. In this case, perturbations to an unstable density structure grow exponentially with time (e.g. Chandrasekhar 1961; Conrad & Molnar 1997). Thus, if $Z$ is the magnitude of a sinusoidal perturbation of wavelength $\lambda$, and $w = dZ/dt$ is its downward speed, both obey

$$\frac{dw}{dt} = qw \qquad \text{and} \qquad \frac{dZ}{dt} = qZ\,, \tag{4}$$

where $q$ is the exponential growth rate.

Conrad & Molnar (1999) non-dimensionalized time and length according to

$$t' = t\,\frac{\rho g\alpha T_0 h}{2\eta_{\mathrm{m}}}\,F_1 \qquad \text{and} \qquad z' = \frac{z}{h}\,, \tag{5}$$

where $\rho$ is the mantle density, $\alpha$ is the thermal expansivity, $g$ is the gravitational acceleration, $T_0$ is the temperature difference across the layer, $h$ is the thickness of the unstable layer and $\eta_{\mathrm{m}}$ is the Newtonian viscosity at the base of the layer. The parameter $F_1$ is a constant that accounts for the temperature dependence of viscosity, termed the 'available buoyancy' by Conrad & Molnar (1999), who showed that $F_1$ is given by the integral through the layer of the thermal buoyancy divided by the viscosity. Because colder portions of the layer are also stronger, the 'available buoyancy' scaling quantifies the portion of the total buoyancy that is sufficiently weak to participate in the gravitational downwelling. Thus, the scaling of time given by eq. (5) applies for cold layers with Newtonian viscosity, and arbitrary dependence of viscosity on temperature.

Using eq. (5) to non-dimensionalize eq. (4) yields an expression for a dimensionless growth rate $q'$, which can be related to the dimensional growth rate, $q$, according to

$$q = \frac{\rho g\alpha T_0 h}{2\eta_{\mathrm{m}}}\,F_1 q'\,. \tag{6}$$

Using numerical experiments, Conrad & Molnar (1999) measured a maximum value of $q' \sim 0.2$ for dimensionless wavelengths close to $\lambda' = \lambda/h = 4$. The combination of eqs (4) and (6) provides an estimate of the downward speed at the bottom of a perturbation growing exponentially with time:

$$w_1 = \frac{dZ}{dt} = \frac{\rho g\alpha T_0 h}{2\eta_{\mathrm{m}}}\,F_1 q' Z\,, \tag{7}$$

where the subscript of $w_1$ refers to the value of the power-law exponent, $n = 1$.

If viscosity is non-Newtonian ($n > 1$), $\eta_{\mathrm{m}}$ decreases as strain rates increase, as shown by eq. (3). For a dense layer undergoing horizontal shortening, strain rates are associated with both horizontal shortening and unstably growing perturbations. For sufficiently small perturbation amplitudes, the strain rates due to shortening are greater and thus determine the effective viscosity of the dense layer. As long as this viscosity remains

constant, perturbations grow exponentially with time and with growth rate given by eq. (6), where the viscosity is given by eq. (3). Once strain rates associated with the growing perturbation begin to dominate those due to shortening, the effective viscosity is affected and growth proceeds super-exponentially. Thus, as suggested by Conrad & Molnar (1997) and confirmed by Molnar *et al.* (1998), perturbations may grow exponentially with time even if viscosity is non-Newtonian, but only if their amplitude is sufficiently small.

### Super-exponential growth

An increase in the amplitude of a growing perturbation causes an increase in strain rates, and thus a decrease in the effective viscosity of a non-Newtonian fluid ($n>1$). This decrease in viscosity causes a density instability to grow super-exponentially with time (e.g. Canright & Morris 1993; Houseman & Molnar 1997). By approximating $\dot{E}\sim w/h$, Houseman & Molnar (1997) obtained an expression for the time-varying viscosity using eq. (3). This leads to an expression for the downward speed, $w_n$:

$$w_n=\frac{dZ}{dt}=\left(\frac{C}{n}\right)^n\left(\frac{\rho_{\mathrm{m}}g\alpha T_0}{B_{\mathrm{m}}}\right)^n hF_nZ^n\,, \tag{8}$$

where $F_n$ is the 'available buoyancy,' which depends on $n$ and the depth dependence of $B$, $B_{\mathrm{m}}$ is the value of $B$ at the base of the unstable layer and $C$ is a dimensionless measure of the rate of growth (Conrad & Molnar 1999). Notice that when $n=1$, eq. (8) reduces to (7) and $C$ is equivalent to $q'$. For $n=3$, measurements of $C$ for different dependences of $B$ on $T$ differ from 0.45 by about 20 per cent (Conrad & Molnar 1999).

Following Houseman & Molnar (1997), Conrad & Molnar (1999) suggested non-dimensionalizing distance and time according to

$$t''=t\left(\frac{\rho g\alpha T_0h}{B_{\mathrm{m}}}\right)^nF_n \qquad \text{and} \qquad z''=z'=\frac{z}{h}\,, \tag{9}$$

where double primes indicate a non-dimensionalization of time for super-exponential growth. Solving for $w_n''$ in terms of $t''$ yields

$$w_n''=\left[C\left(\frac{n-1}{n}\right)(t_{\mathrm{b}}''-t'')\right]^{\left(\frac{n}{1-n}\right)}\,, \tag{10}$$

which indicates super-exponential growth (Houseman & Molnar 1997). Here $t_{\mathrm{b}}''$ is the dimensionless time at which speed becomes infinite and the instability must be detached from the dense layer. By integrating eq. (10), Houseman & Molnar (1997) showed that

$$t_{\mathrm{b}}''=\left(\frac{n}{C}\right)^n\frac{Z_0'^{(1-n)}}{(n-1)}\,, \tag{11}$$

where $Z_0'$ is the perturbation's initial amplitude.

### Horizontal shortening

Horizontal shortening of a layer generates thickening and causes the base of the layer to descend with a speed $w_{\mathrm{s}}=dh/dt$. Incompressibility requires $\dot{\varepsilon}_{xx}=-\dot{\varepsilon}_{zz}=w_{\mathrm{s}}/h$, giving

$$w_{\mathrm{s}}=\frac{dh}{dt}=\dot{\varepsilon}_{xx}h \qquad \text{and} \qquad \frac{dw_{\mathrm{s}}}{dt}=\dot{\varepsilon}_{xx}w_{\mathrm{s}}\,. \tag{12}$$

A comparison to eq. (4) shows that eq. (12) is an expression for exponential growth. In this case, however, it is not the perturbation amplitude $Z$ that grows exponentially with time, but the thickness of the entire layer $h$. The 'growth rate' in this case is simply $\dot{\varepsilon}_{xx}$.

### Diffusion of heat

The cooling of a boundary layer generates the negative buoyancy that drives convective instability. Conductive cooling of a half-space, appropriate for the cooling of oceanic lithosphere, yields a temperature profile given by an error function:

$$T(z)=T_{\mathrm{s}}+T_0\ \mathrm{erf}(-z/h)\,, \qquad \text{where} \qquad h=2\sqrt{\kappa t_{\mathrm{c}}}\,. \tag{13}$$

Here $t_{\mathrm{c}}$ is the time during which the half-space has cooled (e.g. Turcotte & Schubert 1982, pp. 163–167) and $T_{\mathrm{s}}$ is the surface temperature. The rate at which an isotherm at depth $h$ descends can be easily determined by taking the time derivative of $h$:

$$w_{d,v}=\frac{dh}{dt}=\sqrt{\frac{\kappa}{t_{\mathrm{c}}}}=\frac{2\kappa}{h}\,, \tag{14}$$

where the subscripts $d, v$ denote diffusion in the vertical direction.

Diffusion of heat also smoothes, and thus diminishes, the horizontal perturbations in temperature from which instability must grow (e.g. Conrad & Molnar 1997, 1999). Consider perturbations to the background temperature field of the form $\Delta T\sim\cos(kx)$, where $\Delta T$ is the temperature perturbation, $k=2\pi/\lambda$ is the wavenumber and $x$ is the horizontal distance. The horizontal temperature field is subject to the heat conduction equation

$$\frac{\partial\Delta T}{\partial t}=\kappa\left(\frac{\partial^2\Delta T}{\partial x^2}\right)\,, \tag{15}$$

where $\kappa$ is the thermal diffusivity (e.g. Turcotte & Schubert 1982, p. 154). Perturbations decay exponentially with time as

$$\frac{\partial\Delta T}{\partial t}=-\kappa\,\frac{4\pi^2}{\lambda^2}\,\Delta T\,. \tag{16}$$

The wavelength, $\lambda$, should scale with the thickness of the layer, $h$. In addition, the amplitude of a perturbation to an isotherm, $Z$, should be linearly related to the amplitude of horizontal temperature variations, $\Delta T$. Ignoring constants, horizontal thermal diffusion then generates a characteristic rate of

$$w_{d,h}=\frac{dZ}{dt}\sim-\frac{\kappa Z}{h^2}\,, \tag{17}$$

where the negative sign indicates a diminishment of perturbation amplitudes with time.

## NUMERICAL EXPERIMENTS

Numerical experiments, similar to those performed by Conrad & Molnar (1999), can be used to search for the conditions under which each mode of deformation is dominant. I use the finite element code ConMan, which can solve the coupled thermal diffusion and incompressible Navier–Stokes equations for high Prandtl number (King *et al.* 1990). Convective instability is initiated by imposing a temperature field as in eq. (13).

With an assigned thermal expansivity $\alpha$, colder fluid is denser and flows downwards into the underlying warm fluid as the instability grows. Perturbing eq. (13) by applying

$$h(x) = 2\sqrt{\kappa t_c}\sqrt{1 + p\cos(2\pi x/\lambda)}, \quad (18)$$

where $p$ is a constant that specifies the perturbation amplitude, initiates unstable growth. This corresponds to a sinusoidal variation in $t_c$, which imposes a smooth perturbation.

The finite element grid has a depth of $8.27h$ and a width of $\lambda'/2 = 2.07h$. Perturbations with this wavelength grow most rapidly (Conrad & Molnar 1999), and thus should reflect the unstable growth that occurs in a system initially perturbed at all wavelengths. The grid consists of 54 elements in the vertical direction, with 36 elements in the upper half of the box, giving double resolution in the region where most of the deformation occurs. 18 elements in the horizontal direction make each element in the upper half of the box square. This resolution is coarser than that used by Conrad & Molnar (1999), but tests show that measurements of growth rate are only changed by a few per cent. Similarly small changes in growth rate are measured in tests with finer time-step resolution. Following Conrad & Molnar (1999), the length of a time step is chosen to be one-tenth that of the dynamically determined Courant time step.

Horizontal shortening is generated by imposing horizontal velocity boundary conditions along the vertical and top surfaces of the box. Specifically, the left side of the box has zero horizontal velocity, and a horizontal velocity of $-v$ is imposed along the right boundary. On both sides, free slip in the vertical direction is permitted. Along the top surface, the imposed velocity is zero in the vertical direction, and has a horizontal component that tapers linearly from zero on the left to $-v$ on the right. These boundary conditions set up a flow that allows the dense surface layer to thicken according to eq. (12), where $\dot{\varepsilon}_{xx} = 2v/\lambda$. Horizontal shortening could also have been implemented by imposing forces, instead of velocities, on the sides of the box. Although this method more closely resembles lithospheric shortening, which probably involves external forces acting on strong surface plates, it does not specify the location or the rate of thickening, making the resulting deformation more difficult to analyse. In this work, the pattern of shortening is imposed by the velocity boundary conditions, and an assumption is made that external forces could generate this pattern if present. Finally, no stress boundary conditions are imposed along the bottom boundary so that material is not constrained to circulate within the box, which could impede the flow. The box is sufficiently deep, however, that the sinking boundary layer does not begin to feel the bottom of the box as it detaches from the surface layer. Conrad & Molnar (1999) found that, at least initially, a no-stress bottom boundary condition does not affect unstable growth compared to a free-slip condition there. Once cold downwelling approaches the bottom of the box, however, the no-stress condition permits cold fluid to flow out of the box with no resistance. The effects of this flow are discussed below.

Viscosity is non-Newtonian, as described by eq. (3), with power-law exponent $n = 3$. Following Conrad & Molnar (1999), $B$ varies with temperature according to

$$B(T) = B_m \exp\left(\ln(r)\,\frac{T_m - T}{T_0}\right), \quad (19)$$

where the parameter $r$ is the total variation in $B$ across the fluid's temperature range and $T_m$ is the temperature of the underlying fluid. Thus, $B(T_m) = B_m$ and $B(T_s = T_m - T_0) = rB_m$. The temperature dependence of viscosity is altered by varying $r$.

## A COMPARISON OF RATES FOR UNSTABLE GROWTH

A dense layer of non-Newtonian fluid that is undergoing horizontal shortening should exhibit time-dependent behaviour that can be described predominantly by one of the above-mentioned modes of deformation. Two of these modes, uniform thickening of the layer and diffusion of heat in the vertical direction, influence the layer's vertical temperature structure. The rate of uniform downwelling for isotherms at the bottom of a layer experiencing one of these processes is given by $w_s$ or $w_{d,v}$, as defined in eqs (12) and (14). Three processes, exponential growth, super-exponential growth and horizontal diffusion of heat, operate on perturbations to the layer's stratified temperature structure. For each of these modes operating independently, the downward speeds of perturbed isotherms near the bottom of an unstable temperature structure are $w_1$, $w_3$ and $w_{d,h}$, as defined in eqs (7), (8) and (17). In general, all five of these mechanisms should operate simultaneously at different rates, but typically one mode dominates the deformation of a cold, dense layer by causing the layer's isotherms to move most rapidly. Because the above speeds depend on the material properties of the layer, the shortening rate and the amplitude of the perturbations to the layer's temperature structure, the dominant mode should also depend on these quantities, and may change with time as perturbations grow.

In what follows, a series of numerical experiments are used to determine the dominant mode of deformation for various combinations of the relevant parameters. In these experiments, the downward speed of the $T' = 0.9$ isotherm is measured at the location of maximum downwelling for cold layers with a variety of viscosity structures, initial perturbation amplitudes and imposed shortening rates. To apply these experiments generally, dimensionless numbers are constructed by taking ratios of various combinations of the expressions for speed given above. The numerically determined set of parameter values for which a given mechanism deforms isotherms most rapidly can then be expressed as ranges of these dimensionless numbers. Thus, each deformation mechanism is dominating in its own region of dimensionless parameter space, and the boundaries between these regions define 'critical' values of the dimensionless parameters. To determine the dominant mode of deformation for any given layer that is undergoing shortening, one needs only to estimate values for the dimensionless numbers defined below, and then compare these values to the measured 'critical' values. A summary of the various dimensionless parameters and their critical values is given in Table 1.

### Convective instability: unstable growth and thermal diffusion

By studying a layer that is not undergoing horizontal shortening, Conrad & Molnar (1999) determine the basic requirements for convective instability. Their analysis recognizes that horizontal thermal diffusion causes perturbations to an unstable temperature structure to decrease in amplitude with speed $w_{d,h}$ given by eq. (17). If viscosity is effectively Newtonian ($n = 1$),

**Table 1.** Summary of dimensionless quantities (for $n=3$).

| Description of dimensionless quantity | Critical values and dominant mode of growth |
|---|---|
| $Ra_1=\frac{\rho g\alpha T_0 h^3}{\kappa B_m}F_1\dot{\varepsilon}_{xx}^{2/3}$<br>Compares exponential growth and thermal diffusion | $Ra_1 > 100$ exponential growth<br>$Ra_1 < 100$ no growth |
| $Ra_3=\left(\frac{\rho_m g\alpha T_0}{3B_m}\right)^3\frac{h^3Z^2}{\kappa}F_3$<br>Compares super-exponential growth and thermal diffusion | $Ra_3 > 100$ super-exponential growth<br>$Ra_3 < 100$ no growth |
| $P=\frac{\dot{\varepsilon}_{xx}h^2}{\kappa}$<br>Compares mechanical thickening and thickening due to cooling | Applies if $Ra_1<100$ and $Ra_3<100$<br>$P>1$ mechanical thickening<br>$P<1$ thickening due to cooling |
| $\frac{Ra_1}{Ra_3}=3\left(\frac{3B}{\rho g\alpha T_0 Z}\right)^2\frac{F_1}{F_3}\dot{\varepsilon}_{xx}^{2/3}$<br>Compares exponential growth and super-exponential growth | Applies if $Ra_1>100$ or $Ra_3>100$<br>$\frac{Ra_1}{Ra_3}<2$ super-exponential growth<br>$2<\frac{Ra_1}{Ra_3}<100$ exponential growth<br>$\frac{Ra_1}{Ra_3}>100$ mechanical thickening |
| $Z'\frac{Ra_1}{P}=\frac{\rho g\alpha T_0 h}{B_m}F_1\dot{\varepsilon}_{xx}^{-1/3}$<br>Compares exponential growth and mechanical thickening | Applies if $Ra_1>100$ or $Ra_3>100$<br>$Z'\frac{Ra_1}{P}<0.5$ mechanical thickening<br>$0.5<Z'\frac{Ra_1}{P}<5$ exponential growth<br>$Z'\frac{Ra_1}{P}>5$ super-exponential growth |

exponential growth causes fluid to move downwards with speed $w_1$ given by eq. (7). The ratio of these two speeds yields a dimensionless number that is analogous to the Rayleigh number used in thermal convection because it measures convective instability, in this case for a thermal boundary layer:

$$Ra_1=\frac{\rho_m g\alpha T_0 h^3}{2\kappa\eta_m}F_1\sim\frac{w_1}{w_{d,h}}, \tag{20}$$

where the constant $q'$ is ignored in the definition of $Ra_1$. If viscosity is non-Newtonian with power-law exponent $n$, the downward speed is given by $w_n$ in eq. (8). In this case, the relevant dimensionless 'Rayleigh' number becomes

$$Ra_n=\left(\frac{\rho_m g\alpha T_0}{nB_m}\right)^n\frac{h^3Z^{n-1}}{\kappa}F_n\sim\frac{w_n}{w_{d,h}}. \tag{21}$$

Note that if $n=1$, $Ra_n$ becomes $Ra_1$.

Whether perturbations grow unstably or are damped by thermal diffusion depends on the relative values of $w_n$ and $w_{d,h}$, and thus on the parameter $Ra_n$. A large value of $Ra_n$ means that $w_n \gg w_{d,h}$, and unstable growth should dominate. To determine the 'critical' value of $Ra_n$ above which a cold boundary layer becomes convectively unstable, Conrad & Molnar (1999) measured the downward speed of material with a temperature of $T'=T/T_0=0.9$ (near the base of the layer) as a function of time in a series of numerical experiments similar to those described above, but using $\dot{\varepsilon}_{xx}=0$. For $n=1$, the initial slope of a plot of ln $w'$ versus $t'$, made dimensionless using eq. (5), gives the dimensionless exponential growth rate, $q'$. Similarly, if $n>1$, a plot of $w''^{-2/3}$ versus $t''$, where time is non-dimensionalized according to eq. (9), should have a slope of $-C(n-1)/n$, as shown by eq. (10). Varying the viscosity $\eta_m$, or the viscosity coefficient $B_m$ if $n>1$, allows the growth rates $q'$ or $C$ to be determined as a function of $Ra_1$ or $Ra_n$.

Numerical experiments (Conrad & Molnar 1999) show that for large $Ra_1$, growth occurs with dimensionless growth rates close to $q'\sim0.2$. If, however, $Ra_1<1000$, measured values of $q'$ are less than 0.2, and for $Ra_1<100$ they become negative. Negative values of $q'$ indicate that perturbation amplitudes are diminished by the diffusion of heat faster than they can grow. Results are similar for $n=3$, where $C\sim0.45$ for $Ra_3>1000$ and negative for $Ra_1<100$. Thus, the 'critical' value of $Ra_n$ is about 100, at least for $n=1$ and $n=3$. If $Ra_n>100$, unstable growth occurs; otherwise, the layer is stable to convection.

## Horizontal shortening and thermal diffusion

Now consider a layer of fluid with non-Newtonian viscosity and large $B$ such that $Ra_3>100$, and that thickens due to an imposed horizontal strain rate $\dot{\varepsilon}_{xx}$. As described above and by Conrad & Molnar (1999), such a layer should be convectively stable, so that any heat transfer must be due either to advection by the imposed horizontal shortening or to thermal diffusion. Horizontal shortening causes the bottom of a layer to descend with velocity $w_s$, as shown by eq. (12). Isotherms also grow deeper due to cooling from above, at a rate given by eq. (14) as $w_{d,v}$. The ratio of these two rates yields a dimensionless quantity defined here as $P$ because it is similar to a Peclet number, which compares rates of advective and diffusive heat

transport:

$$P = \frac{\dot{\varepsilon}_{xx} h^2}{\kappa} \sim \frac{w_s}{w_{d,v}}, \tag{22}$$

where the factor of 2 is omitted for simplicity. If $P$ is large, boundary layers thicken due to horizontal shortening, but if $P$ is small, they thicken by cooling.

The 'critical' value of $P$ for which the transition between these two types of thickening occurs is determined by first measuring the downward velocity, $w$, of the $T' = 0.9$ isotherm as a function of time for many different values of $P$. Thickening of the layer by horizontal shortening alone causes dimensionless velocity and time to be related according to

$$\frac{w'''}{w'''(t''' = 0)} = \exp t''', \qquad \text{where} \qquad t''' = t\dot{\varepsilon}_{xx}, \tag{23}$$

which is obtained by integrating the expression for $dw_s/dt$ in eq. (12) and where triple primes indicate a non-dimensionalization of time using the strain rate. According to eq. (23), a plot of $\ln(w''')$ versus $t'''$, where $w'''$ is the downward speed of the $T' = 0.9$ isotherm, should have a slope of unity if shortening is dominant. The measured value of this slope is a dimensionless 'growth rate' that is termed $q'''$ here. For a layer undergoing sufficiently rapid shortening that $P$ is greater than about 10, measurements of $q'''$ are close to unity (Fig. 2), which is consistent with uniform thickening. Because these measurements are for a layer that is convectively stable ($Ra_n < 100$), thickening alone must dominate for $P > 10$.

For $P$ less than about 1, $q'''$ increases with decreasing $P$ (Fig. 2), which indicates that growth occurs more rapidly than would be expected for a layer experiencing only mechanical thickening. This is because, for sufficiently small $P$, horizontal shortening is slow enough that isotherms move downwards more rapidly due to cooling than they do because of thickening.

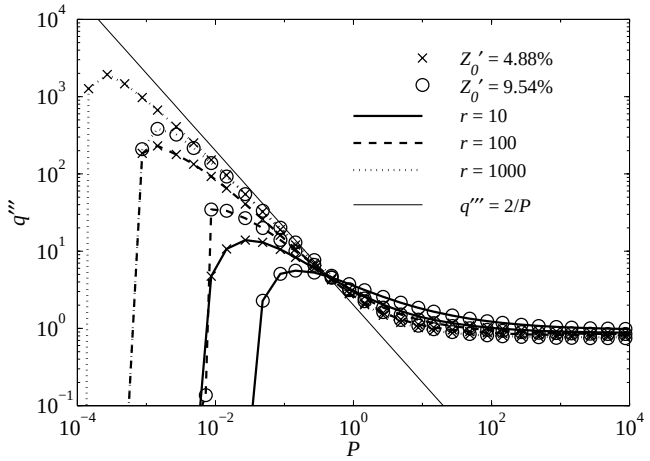


**Figure 2.** Plot of the initial dimensionless 'growth rate,' $q''' = q/\dot{\varepsilon}_{xx}$, as a function of $P$, which is varied by varying $\dot{\varepsilon}_{xx}$. Theory predicts $q''' \sim 1$ if horizontal shortening thickens the layer fastest (observed for $P > 10$) and $q''' \sim 2/P$ (thin solid line) if isotherms deepen due to cooling from above (observed for $P < 1$). At sufficiently small $P$, horizontal thermal diffusion leads to $q''' < 0$ (see text). Growth rates are calculated as described in the text for a set of parameters that yield $Ra_3 = 26\,000 Z_0'^2 F_3$. The maximum value of $Ra_3$ is then 0.7 for $Z_0' = 9.54$ per cent and $r = 10$. The maximum value of $Ra_1$ is 0.7 for this same curve at $P \sim 10^4$. Thus, the layer should only be affected by horizontal shortening and thermal diffusion because both $Ra_1$ and $Ra_3$ are below their critical values for convective instability.

Because the velocity of the *fluid* at the location of a given isotherm is measured and not the vertical motion of the isotherm itself, the measurement of $w'''$ is still that of the thickening layer, given by eq. (12), where $h$ is the depth of the given isotherm. This velocity measurement increases with time, however, because isotherms move downwards due to cooling according to eq. (14), causing $w'''$ to be measured at increasingly deeper locations within the fluid, locations where the fluid velocity given by eq. (12) is greater. The measured value of the downward speed thus changes with time according to

$$\frac{dw}{dt} = \frac{\partial w}{\partial h}\frac{\partial h}{\partial t} = \dot{\varepsilon}_{xx}\frac{2\kappa}{h} = \frac{2\kappa}{h^2} w, \tag{24}$$

where eq. (12) gives $\partial w/\partial h$ and eq. (14) gives $\partial h/\partial t$. By analogy to eq. (4), eq. (24) is an expression for exponential growth with growth rate $q = 2\kappa/h^2$. When made dimensionless using $\dot{\varepsilon}_{xx}$, this growth rate can be simplified to $q''' = 2/P$. This relation approximates the measured values of $q_s'''$ for $P < 1$ (Fig. 2), meaning that vertical thermal diffusion dominates in this range.

At small values of $P$, measured growth rates become negative (Fig. 2). This occurs because the layer is convectively stable ($Ra_1 < 100$ and $Ra_3 < 100$), so that horizontal thermal diffusion causes perturbation amplitudes to decrease with time. If horizontal strain rates, expressed by $P$, are sufficiently small, this leads to negative measurements of the growth rate, as Conrad & Molnar (1999) found for convective instability.

## Convective instability and horizontal shortening

A layer undergoing horizontal shortening may also deform due to gravitational instability. If $Ra_3 > 100$, perturbations grow super-exponentially with time, at least after the effective viscosity is governed by strain rates associated with the growing instability. If background strain rates are larger than those induced by the instability, however, horizontal shortening induces a background Newtonian viscosity given by eq. (3) that should promote initially exponential growth (Molnar *et al.* 1998). For still larger imposed strain rates, uniform thickening may overwhelm either the exponential or the super-exponential growth associated with gravitational instability.

A transition from super-exponential to exponential growth of perturbations is thus expected at some imposed background strain rate. The downward speed of a perturbation growing super-exponentially is given by eq. (8) if $n = 3$ and should be independent of $\dot{\varepsilon}_{xx}$. The downward speed associated with exponential growth is given by eq. (7) and increases with $\dot{\varepsilon}_{xx}^{2/3}$ because the effective viscosity given by eq. (3) for $n = 3$ is proportional to $\dot{\varepsilon}_{xx}^{-2/3}$. The ratio of these two speeds is proportional to the ratio $Ra_1/Ra_3$ and is given by

$$\frac{Ra_1}{Ra_3} = 3\left(\frac{3B}{\rho g \alpha T_0 Z}\right)^2 \frac{F_1}{F_3}\dot{\varepsilon}_{xx}^{2/3} \sim \frac{w_1}{w_3}. \tag{25}$$

Thus, large values of $\dot{\varepsilon}_{xx}$ create large $Ra_1/Ra_3$, which favours exponential growth. Conversely, if $\dot{\varepsilon}_{xx}$ is small, perturbations should grow super-exponentially.

Both types of growth can be demonstrated by plotting $\ln(w')$, where $w'$ is the dimensionless downward speed of the $T' = 0.9$ isotherm, as a function of the dimensionless time, $t'$. As discussed above, if growth is exponential, this curve should be linear, with slope equal to the dimensionless exponential growth rate, $q'$. For $Ra_1/Ra_3 = 10$ the approximately linear initial relationship between $\ln(w')$ and $t'$, with an initial slope

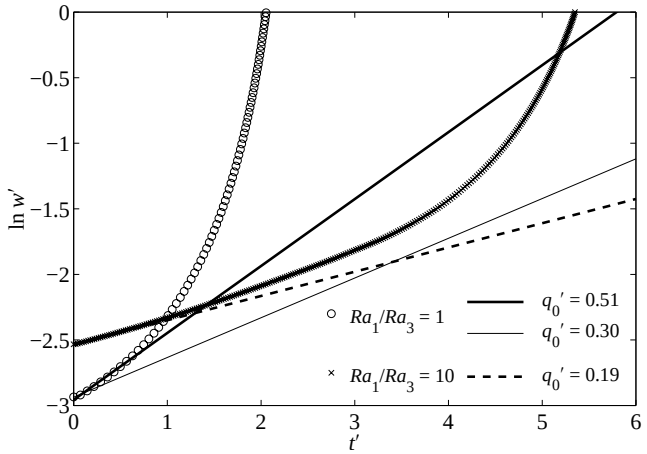


**Figure 3.** Plot of ln $w'$, where $w'$ is the downward speed of the $T'=0.9$ isotherm, versus $t'$ [non-dimensionalized using eq. (5) for exponential growth]. Shown are curves for two choices of $Ra_1/Ra_3$ and for $r=100$ and $Z_0'=9.54$ per cent. For $Ra_1/Ra_3=10$, the initially linear relationship indicates exponential growth with $q'$ close to 0.2, the value measured by Conrad & Molnar (1999). For $Ra_1/Ra_3=1$, the 'instantaneous' growth rate, as measured by the slope of the curve, increases with time. Two methods for measuring the initial instantaneous growth rate, $q_0'$, are shown. A linear fit to the first 10 data points (thick solid line) produces a measurement of $q_0'$ that is too large, but the initial slope of a quadratic fit to the first 20 data points (thin solid line) yields a value that is consistent with predictions made assuming super-exponential growth (see text).

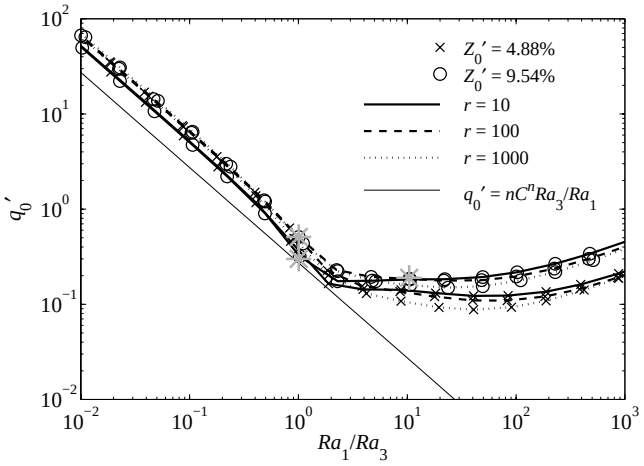


**Figure 4.** Plot of the initial dimensionless growth rate, $q_0'$, as a function of $Ra_1/Ra_3$. Here $q_0'$ is measured as shown in Fig. 3 using a linear fit to the first 10 data points of the curve ln $w'$ versus $t'$. The smallest value of $Ra_3$ is 770 for the $Z_0'=4.88$ per cent and $r=1000$ curve, meaning that the layer is always potentially unstable to super-exponential growth. This type of growth is observed for small strain rates that produce $Ra_1/Ra_3<2$, where theory (see text) predicts super-exponential growth with initially $q_0'=nC^nRa_3/Ra_1$ (thin solid line). For $Ra_1/Ra_3>2$, $q_0'\sim0.2$, as predicted for exponential growth. Thus, for strain rates that are large enough to produce $Ra_1/Ra_3>2$, the background viscosity of the layer is reduced sufficiently so that density perturbations grow unstably and exponentially with time. The grey stars correspond to the measurements made in Fig. 3.

of 0.19 (dashed line, Fig. 3, measured by a linear fit to the first 10 points), agrees with measurements of $q'\sim0.2$ made by Conrad & Molnar (1999) for Newtonian viscosity if $Ra_1>100$ Thus, for $Ra_1/Ra_3=10$, a perturbation initially grows exponentially with time. Later, the slope of this curve in Fig. 3 increases, presumably because super-exponential growth begins to become important.

For $Ra_1/Ra_3=1$, a plot of ln ($w'$) versus $t'$ does not include an initially linear segment, but instead the slope rapidly increases with time (Fig. 3). Growth in this case is super-exponential and the slope of ln ($w'$) versus $t'$ gives a measurement of the 'instantaneous' growth rate at a given time. The above theory predicts the value of this growth rate for a given perturbation amplitude. Taking the time derivative of eq. (8), non-dimensionalizing using the timescale for exponential growth in eq. (5), and then simplifying using the definitions of $Ra_1$ and $Ra_n$ in eqs (20) and (21) yields

$$\frac{dw_n'}{dt'}=nC^n\,\frac{Ra_n}{Ra_1}\,w_n'. \tag{26}$$

Thus, the initial 'instantaneous' slope of a plot of ln ($w'$) versus $t'$, denoted here as $q_0'$, should be equal to $nC^nRa_n/Ra_1$. For $Ra_1/Ra_3=1$, a linear fit to the first 10 data points gives $q_0'=0.51$ (Fig. 3, thick solid line). This value is nearly double the predicted value of $nC^nRa_n/Ra_1=0.27$, calculated using $C=0.45$ (Conrad & Molnar 1999), but it is determined using a rather crude method for fitting a tangent to a set points that are not linear. Instead, measuring the initial slope of a quadratic fit to the first 20 data points gives $q_0'=0.30$ (Fig. 3, thin solid line), which is within 12 per cent of the predicted value.

The transition from super-exponential to exponential growth can now be found by observing how measurements of $q_0'$ depend on $Ra_1/Ra_3$ (Fig. 4). For large $Ra_1/Ra_3$ and exponential growth, the measured initial slope should be constant and equal to $q_0'\sim0.2$ (Fig. 4) (Conrad & Molnar 1999). Although these measurements depend somewhat on perturbation size and begin to increase with increasing strain rate for $Ra_1/Ra_3>100$, measured values of $q_0'\sim0.2$ are evident for $2<Ra_1/Ra_3<100$. For small $Ra_1/Ra_3$, super-exponential growth should dominate even in initial stages. Indeed, for $Ra_1/Ra_3<2$ the measurements of $q_0'$ follow the curve for $nC^nRa_n/Ra_1$ (Fig. 4), as predicted by eq. (26). These measured values are systematically larger, by about a factor of two, than the predicted values. As found for a single example in Fig. 3, this discrepancy is due to the fact that a linear fit to the first 10 velocity measurements yields an overestimate of their true initial growth rate if growth is super-exponential. A linear fit is employed even for super-exponential growth, however, in order to maintain a method for measuring $q_0'$ that is independent of $Ra_1/Ra_3$. Thus, the change in the dependence of $q_0'$ on $Ra_1/Ra_3$ in Fig. 4 can be attributed to the transition between super-exponential and exponential growth, which occurs for $Ra_1/Ra_3\sim2$. This value is independent of $Z_0'$ and the temperature dependence of $B$ (Fig. 4).

At sufficiently rapid background strain rates, uniform thickening of the layer occurs faster than the gravitational instability grows. Thus, another transition, this one from exponential growth to uniform thickening, should occur as strain rates increase. Again, this transition can be found by first taking the ratio of the speeds for mechanical thickening, $w_s$, and exponential growth, $w_1$, which can be simplified to

$$\frac{w_1}{w_s}\sim\frac{Ra_1}{P}\,Z_0'. \tag{27}$$

Thus, layers perturbed with different amplitudes should experience a transition from exponential growth to thickening at different values of $Ra_1/P$.

To see where thickening becomes important, measurements of $q_0'$, the 'instantaneous' initial growth rate discussed above,

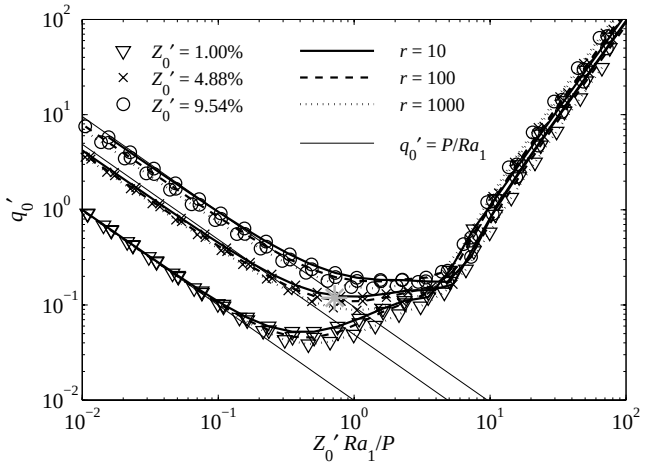


**Figure 5.** Plot of the initial dimensionless growth rate, $q_0'$, made dimensionless using eq. (5), as a function of $Z_0' Ra_1/P$. The results for which $Z_0' Ra_1/P > 5$ are the same as those for which $Ra_1/Ra_3 < 2$ in Fig. 4, where they are attributed to super-exponential growth. Theory predicts (see text) that if growth is controlled by horizontal shortening, $q_0' = P/Ra_1$. This is observed for $Z_0' Ra_1/P < 0.5$ (compare to thin solid lines). For $0.5 < Z_0' Ra_1/P < 5$, a mixture of horizontal shortening and exponential growth causes growth rates to increase towards $q_0' = 0.2$, the value expected for exponential growth. The grey star corresponds to a measurement made in Fig. 6.

are plotted a function of $Z_0' Ra_1/P$ (Fig. 5). If shortening is the most important growth mechanism, the downward speed at the base of a layer is given by $w_s$ in eq. (12). Taking the time derivative of eq. (12), non-dimensionalizing using eq. (5), and simplifying using the definitions of $Ra_1$ and $P$ in eqs (20) and (22) yields

$$\frac{dw_s'}{dt'} = \frac{P}{Ra_1} w_s' . \tag{28}$$

Thus, if the layer grows only by thickening, $q_0' = P/Ra_1$. Measured values of $q_0'$ behave in this way for $Z_0' Ra_1/P < 0.5$ (Fig. 5) for the three different initial perturbation amplitudes. For $Z_0' Ra_1/P > 0.5$, measured growth rates trend towards $q' \sim 0.2$. For small initial perturbations such as $Z_0' = 0.01$, growth rates may be smaller than $q' \sim 0.2$ even for $Z_0' Ra_1/P > 0.5$ (Fig. 5), indicating that horizontal shortening still influences growth.

The transition between exponential and super-exponential growth, determined from Fig. 4 to occur at $Ra_1/Ra_3 \sim 2$, can also be represented in terms of $Z_0' Ra_1/P$ and observed in Fig. 5. By solving for the strain rate at which $Ra_1/Ra_3 \sim 2$ and inserting this expression into the definition of $Z_0' Ra_1/P$ given in Table 1, it is possible to rewrite $Ra_1/Ra_3 \sim 2$ as $Z_0' Ra_1/P \sim 3.67 F_1 \sqrt{F_1/F_3}$. Using the values of $F_1$ and $F_3$ given by Conrad & Molnar (1999), the transition from exponential to super-exponential growth can be estimated to occur at $Z_0' Ra_1/P \sim 5$. This transition is evident in Fig. 5, and is, coincidentally, nearly independent of the temperature dependence of $B$ across the layer.

### Summary

Three dimensionless quantities, $Ra_1$, $Ra_n$ and $P$, together with the initial dimensionless perturbation size, $Z_0'$, can be used to determine the mode of deformation that occurs in a cold thickening boundary layer with non-Newtonian viscosity and power-law exponent $n = 3$ (Table 1). If $Ra_3 > 100$, the instability may grow super-exponentially, but only if imposed strain rates, $\dot{\varepsilon}_{xx}$, are small enough that $Ra_1/Ra_3 < 2$ (Fig. 4), or alternatively $Z_0' Ra_1/P > 5$ (Fig. 5). If the imposed strain rate is large enough that $Z_0' Ra_1/P < 0.5$ (Fig. 5), or alternatively $Ra_1/Ra_3 > 100$ (Fig. 4), mechanical thickening of the layer dominates the downward advection of isotherms (Fig. 5). Intermediate imposed strain rates lead to exponential growth of perturbations, as long as $Ra_1 > 100$.

## TRANSITIONS BETWEEN MECHANISMS OF INSTABILITY

The dimensionless quantities $Ra_1$, $R_3$ and $P$ depend on the layer thickness $h$, and thus increase as the layer thickens with time. The measure of instability $Ra_3$ also increases as gravitational instability grows because it depends on the perturbation amplitude $Z$. As a result, an unstable layer should experience transitions between different types of deformation as increases in $h$ and $Z$ cause $Ra_1$, $Ra_3$ and $P$ to encounter the 'critical' values described above and in Table 1.

As an example, consider convective instability at the base of a layer perturbed initially with amplitude $Z' = 4.88$ per cent, $r = 100$ and choices of $\dot{\varepsilon}_{xx}$ and other parameters such that $Z' Ra_1/P \sim 0.7$. As noted in Fig. 5 and shown by a plot of ln ($w'$) versus $t'$ (Fig. 6a), such a layer undergoes a combination of Rayleigh–Taylor growth and horizontal shortening such that

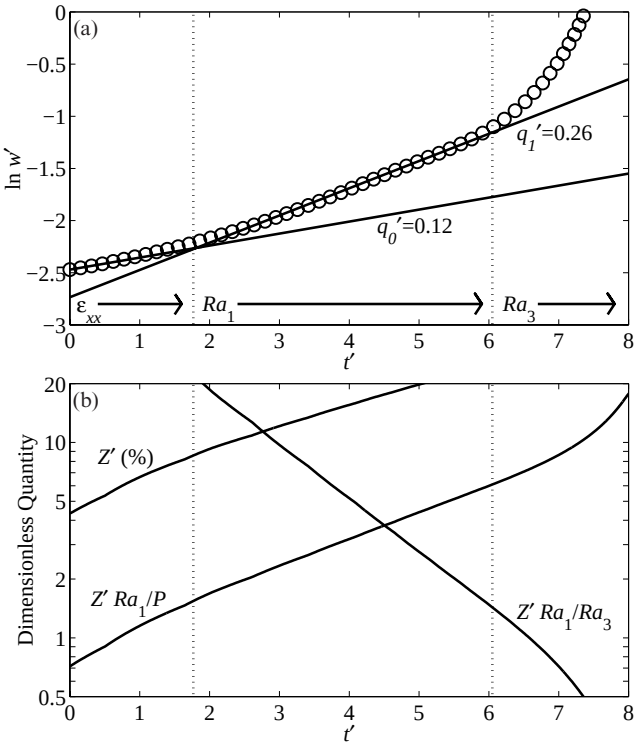


**Figure 6.** Plot of (a) ln $w'$ and (b) the dimensionless quantities $Z'$, $Z' Ra_1/P$ and $Ra_1/Ra_3$ as a function of time [made dimensionless using the timescale for exponential growth in eq. (5)] for a layer with initial values of $Ra_1$, $Ra_3$ and $P$ of 800, 10 and 50, respectively, and for $r = 100$ and $Z_0' = 4.88$ per cent. The changes in slope in (a) suggest that growth is initially dominated by the imposed thickening, then by exponential growth of perturbations, and then by super-exponential growth of these perturbations. The transitions between the various types of growth are approximately predicted by the values of $Z'$, $Z' Ra_1/P$ and $Ra_1/Ra_3$ in (b) passing critical values that are indicated as changes in slopes in Figs 4 and 5.

$q' = 0.12$, where time is made dimensionless using eq. (5). This value is smaller than the value of $q' \sim 0.2$ appropriate for purely exponential growth. As discussed above and shown in Fig. 5, however, $q' < 0.2$ for initial perturbation amplitudes that are sufficiently small because shortening still influences growth. Thus, in the example shown in Fig. 6(a), isotherms are initially advected downwards in part by uniform thickening of the layer.

As the perturbation amplitude $Z'$ increases with time due to Rayleigh–Taylor growth, the quantity $Z'Ra_1/P$ also increases, making deformation of the layer less influenced by mechanical thickening (Fig. 5). In fact, the transition to exponential growth occurs as the perturbation amplitude nears $Z' \sim 10$ per cent and $Z'Ra_1/P$ nears 1.4 (Fig. 6b), seen also in the change in slope near $t' = 2$ (Fig. 6a). The new measured growth rate of $q' = 0.26$ is larger than expected for exponential growth. Because the layer has thickened by about 30 per cent before exponential growth becomes dominant, however, the thickness $h$ used in eq. (5) to make time dimensionless should be increased by a factor of 1.3, making the value of 0.26 consistent with the predicted dimensionless growth rate of $q' = 0.2$ (Conrad & Molnar 1999). When perturbation amplitudes become sufficiently large that $Ra_3 > 100$ and $Ra_1/Ra_3 < 2$ (or $Z'Ra_1/P > 5$), super-exponential growth of perturbations is faster than exponential growth. This transition is evident by the acceleration of growth that occurs for $t' > 6$ (Fig. 6a), which is the time both $Z'Ra_1/P$ and $Ra_1/Ra_3$ reach their predicted critical values of 5 and 2 (Fig. 6b).

Thus, for a thickening unstable layer, the dominant mode of deformation progresses from exponentially increasing mechanical thickening to faster exponential growth of a gravitational instability and finally to still faster super-exponential growth of this instability. Depending on initial conditions, these three types of deformation will evolve from one to the next as the layer thickens and perturbations grow. The scaling analysis developed above for an initially perturbed layer can be used to predict the approximate time-dependent evolution of a thickening unstable layer that experiences transitions between different styles of thickening and growth as it evolves.

## THE EVOLVING THERMAL STATE OF AN UNSTABLE LAYER

If mechanical thickening of mantle lithosphere generates convective instability, the lithosphere's low-viscosity basal portion will be removed in an event whose time dependence is described above. Previous studies of convective instability (e.g. Conrad & Molnar 1999; Molnar *et al.* 1998) extrapolate the analysis for a single downwelling event to the ongoing convective erosion of a layer afterwards. Horizontal shortening at the surface, however, should persist even after the initial instability, and thus should affect any continued downwelling that may occur. To study the evolution of mantle lithosphere after its base has been convectively removed, calculations similar to those described above are extended for times beyond this initial event.

### Additional numerical calculations

In the lithosphere, shortening, and therefore convective instability caused by shortening, occurs at convergent zones between large plates of nearly constant thickness. To consider durations of convergence long enough to allow large finite shortening, I extend the width of the finite element grid to $6.20h$, three times that used in the calculations above. The wider grid generates instability further than the imposed boundary conditions that generate shortening, and thus should diminish the influence of these boundary conditions on the evolution of the shortening region. Shortening is permitted only in the left one-third of the grid by adding uniform velocity boundary conditions to the top surface of the rightmost two-thirds of the grid. Thus, at the surface, the horizontal velocity tapers uniformly from zero to $-v$ on $0 < x' < 2.07$ and is equal to $-v$ on $2.07 < x' < 6.20$. Other boundary conditions are the same as those used above.

The imposed horizontal shortening causes the unstable layer to thicken at a rate that can be expressed by $P$ using eq. (22) as a multiple of the thermal diffusion timescale. Perhaps a more meaningful expression for the thickening rate is the time for a layer's thickness to increase by 100 per cent. In these calculations, a doubling of layer thickness can be achieved by collapsing a region of width $2L$ into a region of width $L$, which corresponds to horizontal shortening of 50 per cent. If $L$ is the width of the shortening region and material is brought into this region with velocity $v$, then the horizontal strain rate is $\dot{\varepsilon}_{xx} = v/L$ and 100 per cent thickening is achieved after a time $t_{100} = L/v = 1/\dot{\varepsilon}_{xx}$. Using eq. (22), $t_{100}$ can be written in terms of $P$,

$$t_{100} = \frac{1}{\dot{\varepsilon}_{xx}} = \frac{h^2}{P\kappa} . \tag{29}$$

Later, it will be useful to make time non-dimensional using the timescale for exponential growth. Applying eq. (5) and simplifying yields

$$t'_{100} = \frac{Ra_1}{P} . \tag{30}$$

Values for $P$ and $Ra_1$ are given below so that $t'_{100}$ can be calculated using eq. (30).

16 calculations are performed, for four different temperature dependences of viscosity, given by values of $r$ of 1, 10, 100 and 1000, and for four different shortening rates, which yield values of $P$ of 1.5, 4.8, 15 and 48. Because the stability parameter $Ra_1$ depends on strain rate, as shown by eqs (20) and (3), layers with larger values of $P$, and thus larger strain rates, have larger $Ra_1$ and are convectively more unstable. To study layers that are inherently stable when subject to low shortening rates, but that become unstable when shortening rates increase, the strength parameter $B_m$ is chosen so that a layer shortening with $P = 4.8$ has a value of $Ra_1$ near the critical value of 100. Because layers with larger $r$, and therefore smaller 'available buoyancy' parameter $F_1$, have a diminished tendency towards convective instability (as shown by eq. 20), the chosen values of $B_m$ are smaller for layers with larger $r$. Thus, despite differences in $r$, layers are equally unstable at a given shortening rate. The stability parameter $Ra_1$ is thus varied only by changing the shortening rate, which is specified here by a change in $P$.

Because horizontal shortening is only imposed between $x' = 0$ and 2.07, thickening in this region generates a perturbation to the initially unperturbed error function temperature profile. This perturbation then should grow unstably, either exponentially with time if shortening is sufficiently rapid that $Ra_1 > 100$, or super-exponentially with time once this perturbation becomes large enough that $Ra_3 > 100$. Either way, localized thickening eventually leads to a perturbation that grows unstably. This initial downwelling eventually removes the basal portion of the

layer, as shown for $r=100$ by the locations of isotherms in Fig. 7 (black lines). Typically, downwelling persists following the initial removal event, and continues to remove both cold material from the upper reaches of the surface layer and new material that is brought in from the side. This downwelling appears to be a permanent feature and eventually reaches a steady state in which it removes all new cold material that is brought in by the imposed horizontal shortening (Fig. 7, grey lines).

### The evolution of downwelling

To study the instability's development over time, I record the locations and downward speeds of the nine isotherms between $T'=0.1$ and $T'=0.9$ on the left side of the box, where the instability is a maximum. I also record the depths of these isotherms as they are advected into the right-hand side of the box. The amplitude of the perturbation to each isotherm, $Z'$, can be measured by taking the difference in an isotherm's depth between the left- and right-hand sides of the grid, and then normalizing this quantity by the original depth of that isotherm. To determine the fraction of the downward speed that is not due to the initially imposed velocity field associated with horizontal shortening, the initial speed of material containing a given isotherm is subtracted from its measured value. Because the layers are initially unperturbed, this initial speed should result almost entirely from horizontal shortening. The velocity that remains, termed $w'_{\rm corr}$ here, must be associated with either gravitational instability or the acceleration of mechanical thickening beyond its initial rate (remember that $w_s$ in eq. (12) grows exponentially with time).

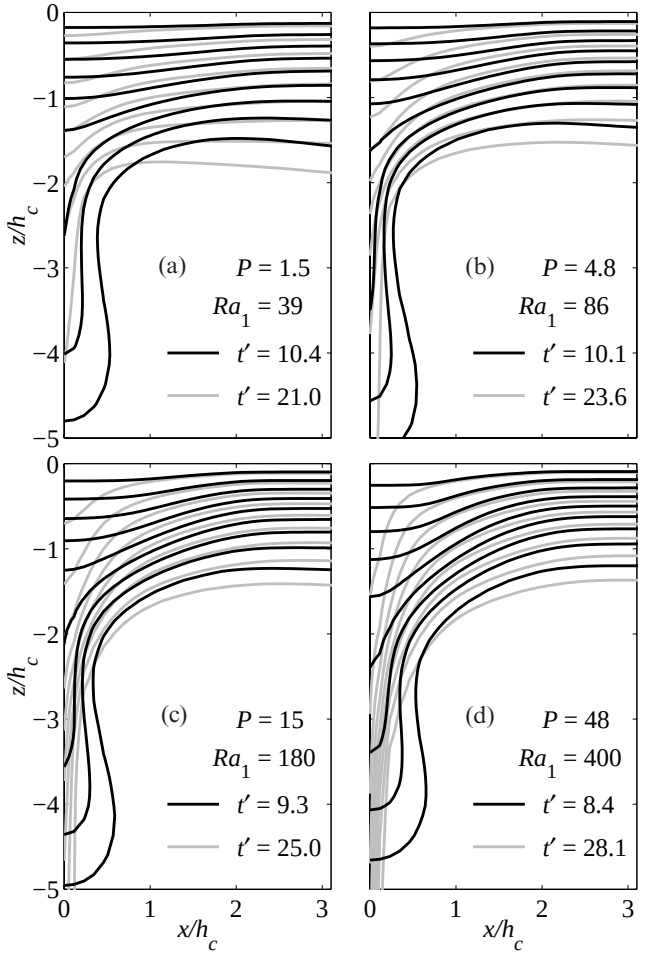


**Figure 7.** Profiles of temperature for a convective instability growing from a thickening thermal boundary layer with temperature-dependent, non-Newtonian viscosity for which $n=3$ and $r=100$. Only the left half and the upper 60 per cent of the entire finite element calculation is shown. Shown are isotherms for $T'=0.1$–$0.9$, with colder temperatures closer to the surface. Sets of isotherms for different shortening rates are shown in (a)–(d), where the difference in shortening rates is parametrized by $P$, but also affects $Ra_1$ by changing the background viscosity of the layer. In each case, two times are shown, where time is non-dimensionalized using the timescale for exponential growth given by eq. (5). The dark contours show a time during the super-exponential phase of the instability in which a 'blob' of material is rapidly descending into the lower half-space. The light contours show the instability at the end of the calculation, when cold material is flowing downwards from the base of the instability at a nearly steady rate.

A comparison of the expressions for $w_1$ and $w_n$ in eqs (7) and (8) shows that if gravitational instability dominates, a plot of ln ($w'_{\rm corr}$) versus ln ($Z'$) should yield a linear relationship with slope equal to the power-law exponent, $n$, that depends on the style of growth: $n=1$ for exponential and $n>1$ for super-exponential growth (Molnar *et al.* 1998). If mechanical thickening dominates, subtracting the initial velocity from eq. (12) yields $w_{\rm corr}=\dot{\varepsilon}_{xx}Z$ if $h(t)=h(t=0)+Z(t)$. This relation should, like exponential growth, yield a slope of unity in a plot of ln ($w'_{\rm corr}$) versus ln ($Z'$). Such a plot (Fig. 8) shows an initial slope near unity for all of the isotherms, indicating exponential growth of perturbations or mechanical thickening. For the hotter isotherms, a change in slope indicates a transition to super-exponential growth of perturbations (slope of $m=n=3$). For all of the calculations shown in Fig. 8, the dimensionless quantity $Z'Ra_1/P>0.5$ for $Z'>6$ per cent ($\ln(Z')>-2.8$). This implies that exponential growth (rather than horizontal shortening) dominates prior to the transition to super-exponential growth, at least for the hotter isotherms.

### The thermal state after initial instability

The amount of material removed by the initial instability can be estimated by observing the number of isotherms that participate in the initial downwelling in Fig. 7. For example, the bottom three isotherms are clearly involved in the downwelling for the slowest shortening rate (Fig. 7a). A fourth isotherm appears to join the instability for faster shortening (Fig. 7d). Another way of determining how much material is initially removed is to estimate how many isotherms change their slopes from $m=1$ to $m=3$ in Fig. 8, and thus demonstrate super-exponential growth of perturbations. In each of the four cases shown, the hotter four isotherms display changes in slope. The initial removal event is also evident in a plot of the depth of each isotherm as a function of time (Fig. 9), and it is clear that between three and four isotherms are removed by it.

A more quantitative estimate of the amount of material removed by the initial instability can be obtained by examining the distribution of isotherms at the removal time in Fig. 9. In particular, the ratio of each isotherm's depth at a given time to its initial depth defines a 'thickening factor' that can then be used to compare the relative deflections of different isotherms at various times. At the removal time, defined here to be the time in which the $T'=0.9$ isotherm first encounters the bottom boundary of the finite element grid, isotherms are typically

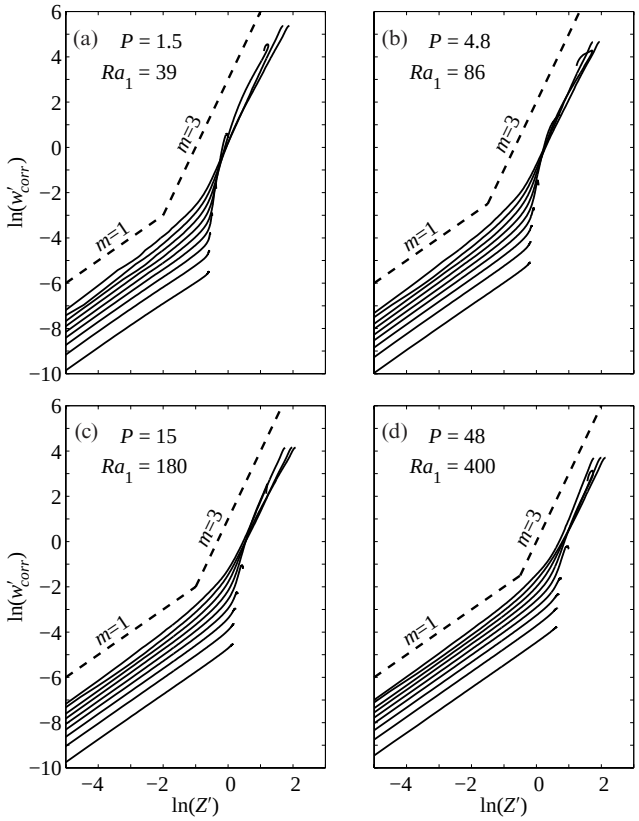


**Figure 8.** A plot of ln ($w'_{corr}$) as a function of ln ($Z'$) for each of the nine isotherms (solid lines, $T'=0.1$–$0.9$, colder isotherms have smaller initial velocities) and for the four calculations shown in Fig. 7 (a–d). Only times before the $T'=0.9$ isotherm encounters the bottom of the box are shown. Theory predicts (see text) a slope of $m=1$ if either exponential growth or horizontal shortening controls growth and $m=3$ if perturbations grow super-exponentially. Dashed lines with slopes of 1 and 3 are shown for comparison.

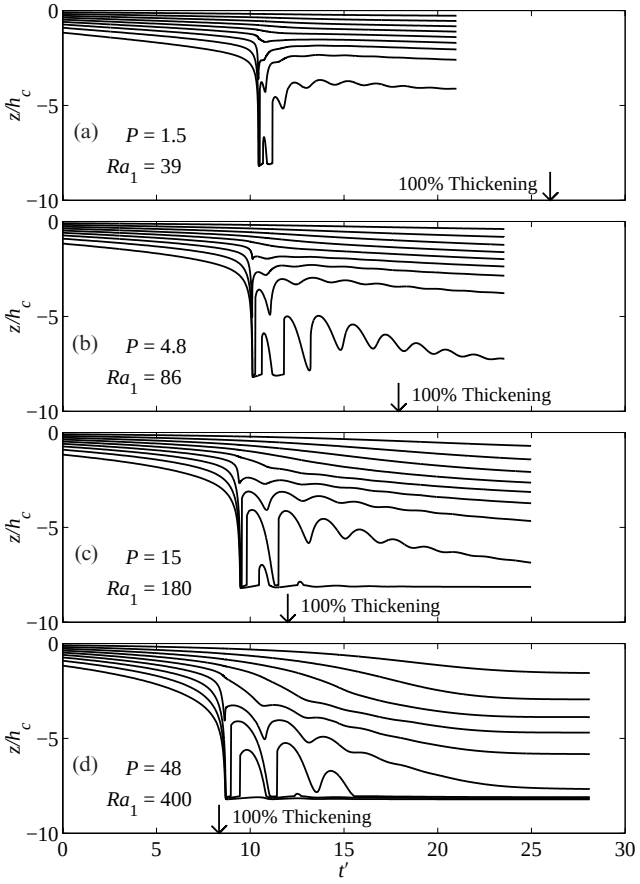


**Figure 9.** A plot showing the depth of each of the nine isotherms ($T'=0.1$–$0.9$, colder isotherms are closer to the surface) as a function of time [made dimensionless using the timescale for exponential growth in eq. (5)] for the four calculations shown in Fig. 7 (a–d). In each case, the super-exponential growth phase is evident as the bottom isotherms plunge deeply into the lower half-space, eventually descending through the base of the grid at $z'=8.27$. These isotherms then begin a period of oscillatory behaviour while the shallower isotherms continue to be drawn downwards. Also shown for each case is the dimensionless time at which the layer would have thickened by 100 per cent in the absence of convective instability. This time corresponds to 50 per cent shortening at the surface and is given by eq. (30) as $t'_{100}=Ra_1/P$.

separated into two groups. Colder isotherms subside steadily with time (Fig. 9) and typically deepen by a factor of less than about 3 by the time of the removal event. Hotter isotherms that actively participate in this event penetrate deeply into the box, which causes them to grow deeper by factors of greater than about 7, a quantity limited by the box depth (Fig. 9). The isotherm that delineates the boundary between these two types of behaviour can be defined as the temperature of material for which an arbitrarily chosen thickening factor of 5 applies (Fig. 10). The factor of 5 is midway between the values of 7 and 3 estimated for isotherm 'removal' and 'non-removal,' but tests show that choosing 4 or 6 gives similar results.

Thus, the approximate temperature of the coldest material that participates in the initial removal event is shown in Fig. 10. Because at least some warming must occur as the cold downwelling fluid descends, the temperatures shown in Fig. 10 can be considered an upper bound on the original temperature of this material. For example, the $T'\sim0.7$ isotherm is removed for $r=100$ and slow shortening rates (Fig. 10), an estimate that is supported by comparing the deflection of the $T'\sim0.7$ isotherm to that of the other isotherms in Fig. 9(a). Thus, in this case, *at least* the warmest 30 per cent of the original layer participates in the initial removal event. The cut-off temperature for removal (Fig. 10) is highly dependent on the temperature dependence of the viscosity coefficient, $r$, with nearly the entire layer being initially removed in the constant $B$ case ($r=1$), and only the bottom few isotherms being removed if $r=1000$. As found above for $r=100$, the amount of material removed in this initial removal event does not depend strongly on the rate of shortening. This is due to the domination of the initial removal event by super-exponential growth, which, unlike exponential growth, does not depend on the shortening rate. Thus, the shortening rate should not affect the amount of material removed in this *initial* instability, provided this rate is large enough to generate instability.

### The thermal state after prolonged thickening

Because these calculations extend beyond the initial instability, they can be used to examine deformation of the unstable layer after the initial removal event. As the initial downwelling passes through the base of the finite element grid, the negative thermal buoyancy associated with the downwelling isotherms is suddenly

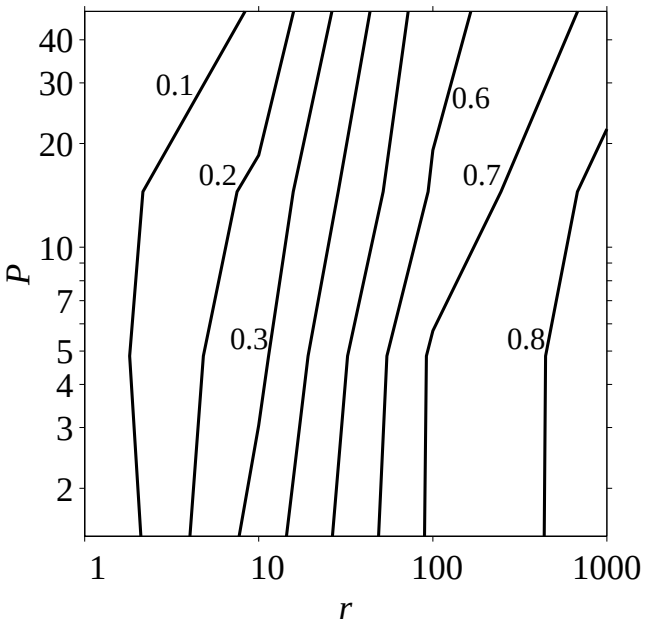


**Figure 10.** A plot showing the approximate temperature of the coldest material removed by the initial super-exponential removal event (see text) as a function of shortening rate (expressed by $P$) and the temperature dependence of viscosity (expressed by $r$). It is evident that a greater portion of the layer is initially removed if viscosity is only weakly temperature-dependent (smaller $r$) and that the shortening rate has little effect on the amount of material removed in this initial event.

removed, which causes these isotherms to retreat rapidly. This response is typically followed by another advance of downwelling, and oscillatory behaviour develops (Fig. 9) until it is damped into a steady-state downwelling flow (Fig. 7). Such oscillatory behaviour is an artefact of the no-stress boundary conditions at the base of the box, which led to a premature detachment of cold downwelling fluid from the surface layer. Because these oscillations are minimal for the material that remains in the surface layer (Fig. 9) and because they are eventually damped, the no-stress boundary conditions should only affect the details of the large-amplitude removal of the initial downwelling, which we do not study here.

Several colder isotherms that do not participate in the initial removal event are eventually drawn into the continued downwelling flow that follows (Fig. 7). This behaviour is the expected result of mechanical thickening of the cold part of the layer. The velocity boundary conditions force cold fluid into the right side of the finite element grid and out through its bottom. If the cold surface layer is in thermal steady state, this cold fluid must be removed from the layer by the persistent downwelling. In this light, it is not surprising that increased shortening rates are associated with a more substantial downwelling that penetrates deeper into the underlying fluid. Although these persistent downwellings are generated by shortening, they are facilitated by the inherent gravitational instability of this material, which prevents the surface layer from thickening into an overly unstable condition from which another transient instability can develop. Thus, the persistent downwellings that follow prolonged shortening are part of the steady-state behaviour of a shortening layer.

In the Earth, however, shortening cannot be expected to continue indefinitely. If shortening ceased, some, at least, of the material protruding into the asthenosphere would presumably become unstable, detach, and then be replaced by hotter material. The amount of material that might be removed can be estimated by measuring the temperature of the coldest material that protrudes deeper than the original depth of the $T'=0.9$ isotherm, taken to represent the base of the unstable layer. These temperatures are shown in Fig. 11 for a downwelling in thermal steady state. It is clear that colder material is removed from more rapidly shortening layers (large $P$), but that the temperature of material removed is independent of the temperature dependence of viscosity.

### The thermal state after 50 per cent shortening

Geological observations in severely shortened regions such as Tibet indicate that the total amount of horizontal shortening can reach 50 per cent (shortening by a factor of two) (Le Pichon *et al.* 1992; Molnar *et al.* 1993). Horizontal shortening of this magnitude can be accommodated by a doubling of crustal thickness (100 per cent thickening) in the shortening region, which generates significant buoyancy that resists further crustal thickening. This resistance causes the region of active shortening to migrate to undeformed adjacent regions once horizontal shortening has reached about 50 per cent (e.g. England & Houseman 1986; England & Searle 1986; Molnar & Tapponnier 1978). If the amount of horizontal shortening is limited to 50 per cent, the amount of time that dense mantle lithosphere is exposed to the destabilizing effects of horizontal shortening is also limited. In this case, the persistent downwellings discussed above might not penetrate as deeply as they would have if allowed to grow indefinitely.

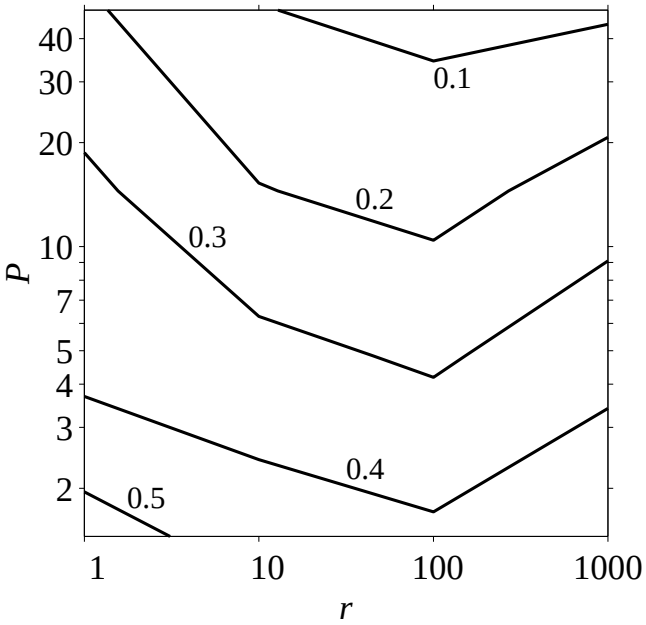


**Figure 11.** Similar to Fig. 10, but showing thermal properties of the steady-state persistent downwelling that removes material added to the layer by shortening. Here the temperature of downwelling material at a depth equal to that of the original position of the $T'=0.9$ isotherm is shown. If shortening were to stop at this point, material hotter than that shown here would presumably be removed. It is clear that the persistent downwelling advects cold material deeper into the mantle if the shortening rate is higher (larger $P$), and that the temperature dependence of viscosity is of lesser importance.

Because the dimensionless time to the initial removal event is a constant value of about 8, 50 per cent shortening occurs well after the initial removal event for a slowly shortening layer (Fig. 9a), but the two may be nearly simultaneous if shortening is rapid (Fig. 9d). Thus, for the shortening rates studied, 50 per cent shortening typically occurs sometime after the initial removal event, but before the persistent downwelling has grown to its full extent. To characterize the thermal state of the persistent downwelling at the time of 50 per cent shortening, the temperature of the coldest material at the original depth of the $T'=0.9$ isotherm is again recorded, this time at the dimensionless time $t'_{100}$. The result (Fig. 12) shows that this temperature is generally hotter at the time of 50 per cent shortening than it is after prolonged shortening (compare to Fig. 11), particularly at large strain rates. In fact, the increased temperatures at large $P$ cause the dimensionless temperature to have a nearly uniform value between 0.3 and 0.4 (Fig. 12). Thus, if convergence slows after shortening an unstable layer by 50 per cent, the hottest 60–70 per cent of downwelling fluid should be removed, a value independent of the shortening rate and the temperature dependence of viscosity.

## APPLICATION TO THE LITHOSPHERE

The above analysis shows that several styles of deformation are possible for a dense layer undergoing horizontal shortening, and that the particular style that a layer chooses depends on the values of the dimensionless quantities $Ra_1$, $Ra_3$, $P$ and $Z'$. This analysis can now be applied to the mantle lithosphere to determine the types of deformation that are possible as a result of shortening, and to characterize the changes to the lithospheric structure that may result from this deformation. To do this, parameter values relevant to the lithosphere must be estimated. These include $\rho_m=3300$ kg m$^{-3}$, $g=9.8$ m s$^{-2}$, $\alpha=3\times10^{-5}$ K$^{-1}$ and $\kappa=10^{-6}$ m$^2$ s$^{-1}$. If the mantle lithosphere varies in temperature between $T_s=800$ K at the Moho and $T_m=1600$ K at its base, the temperature variation across the potentially unstable mantle lithosphere is $T_0=T_m-T_s=800$ K.

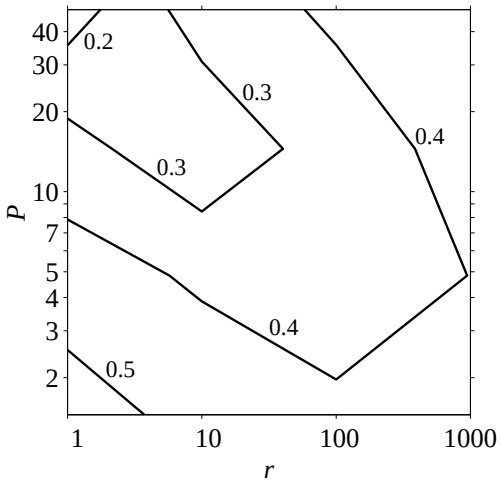


**Figure 12.** Similar to Fig. 11, but showing measurements taken at $t_{100}$, the time for 100 per cent thickening (or 50 per cent horizontal shortening) to occur. In this case, the temperatures shown depend only weakly on both the shortening rate given by $P$ and the viscosity variation given by $r$.

The rheology of mantle lithosphere is thought to be characterized by diffusion creep, for which $n=1$, at stresses lower that 0.1–1 MPa, and by dislocation creep, for which $n=3$ to 3.5, at higher stresses (Karato *et al.* 1986). Convective instability should be accompanied by stresses greater than this, favouring dislocation creep. Hirth & Kohlstedt (1996) proposed that the mantle is 'wet' below 60–70 km depth, for which Karato *et al.* (1986) deduced a power-law exponent of $n=3$, an activation energy of $Q=420$ kJ mol$^{-1}$ and a pre-exponential factor of $A=1.9\times10^{-15}$ Pa s$^{-3}$ for olivine. Using these parameter values, Conrad & Molnar (1999) estimated $B_m=1.9\times10^9$ Pa s$^{1/3}$. Hirth & Kohlstedt (1996), however, assigned $n=3.5$ to wet olivine. The considerable uncertainty associated with Conrad & Molnar's (1999) estimate of $B_m$ is accommodated here by using $n=3$ and allowing $B_m$ to vary.

The 'available buoyancy' parameter $F_n$ accounts for the temperature dependence of $B$ for a given temperature profile in a layer. Conrad & Molnar (1999) estimated its value for wet dislocation creep by assuming an activation energy of $Q=420$ kJ mol$^{-1}$. They found $F_3=1.3\times10^{-4}$ for an error function temperature profile. If the strain rates associated with horizontal shortening control the effective viscosity of the layer, this viscosity is constant with perturbation amplitude, meaning that the power-law exponent $n=1$ is applicable. Following Conrad & Molnar (1999), $F_1=5.7\times10^{-2}$ for the error function temperature profile, which is slightly larger than that estimated by Conrad & Molnar (1999) for $n=1$, because their study uses parameters for diffusion creep without horizontal shortening. If the temperature profile is not that of an error function, estimates of the 'available buoyancy' should be different from those assumed here. This uncertainty is acceptable, however, because it can be absorbed by the uncertainty associated with the strength parameter $B_m$.

As described above, the values of $Ra_1$, $Ra_3$ and $P$ can be used to determine which of the above-described mechanisms should dominate lithospheric deformation. In particular, their 'critical' values (Table 1) delineate transitions between different styles of thickening and growth. By plotting the locations of these transitions as a function of parameters that can vary, a 'phase diagram' can be constructed that shows the dominant style of growth in different regions of the space defined by the variable parameters. An example diagram (Fig. 13) shows the typical locations of boundaries between the four deformation styles, or 'phases,' in the space defined by the strength parameter $B_m$ and the time $t_{100}$, for 100 per cent thickening to occur, which defines the strain rate according to eq. (29). In this case, if both $Ra_3<100$ and $Ra_1<100$, the layer is convectively stable, with mechanical thickening (MT) dominating if $P>1$ and thickening by thermal diffusion (TD) dominating otherwise. If $Ra_1>100$, horizontal shortening still dominates if $Z'_0Ra_1/P<0.5$, otherwise perturbations grow exponentially (EG) with time for $Ra_1/Ra_3>1$ and super-exponentially (SEG) otherwise. The locations of these boundaries relative to dimensional values of $B_m$ and $t_{100}$ depend on the parameters used to calculate $Ra_1$, $Ra_3$ and $P$. As a result, diagrams are constructed by plotting the locations of these 'critical' values as functions of $B_m$ and $t_{100}$ for the lithospheric parameters given above, perturbation amplitudes of $Z'_0=10$ per cent (Fig. 14) and $Z'_0=50$ per cent (Fig. 15), and layer thicknesses of $h=25$, 50, 100 and 200 km (a–d in Figs 14 and 15).

The boundaries between dominating styles of thickening or unstable growth change as the mantle lithosphere thickens,

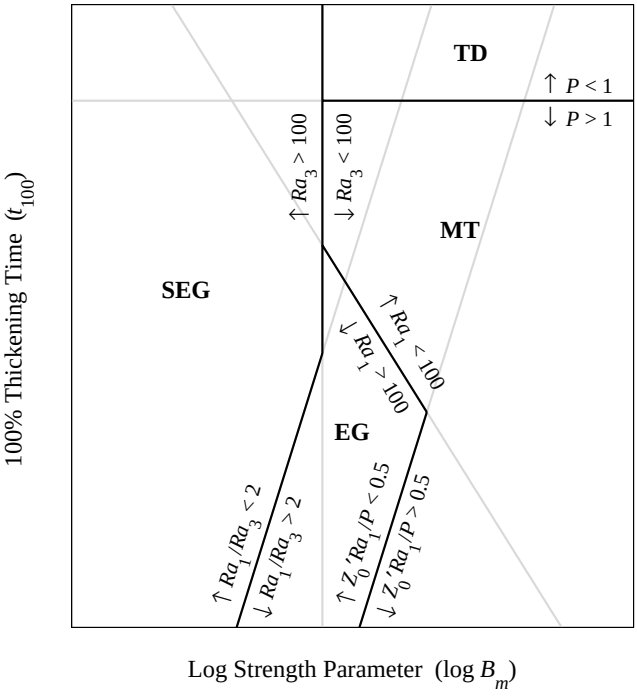


**Figure 13.** A cartoon of a 'phase diagram' that shows the dominant style of thickening or growth (the 'phases') as a function of the strength parameter $B_m$ and the time, $t_{100}$, for 100 per cent thickening (or 50 per cent horizontal shortening) to occur. Here, $t_{100}$ defines the background horizontal strain rate, as in eq. (29). The boundaries between each of the four regions are determined by the 'critical' values associated with $Ra_1$, $Ra_3$ and $P$ summarized in Table 1: $Ra_1=100$, $Ra_3=100$, $P=1$, $Ra_1/Ra_3=2$ and $Z_0'Ra_1/P=0.5$. For each line, arrows show the direction in which a quantity increases or decreases away from the line. Light lines show portions of these lines that are not relevant to determining the stability of a given mode. The four mechanisms include thickening by thermal diffusion (denoted TD), mechanical thickening associated with horizontal shortening (denoted MT), exponential growth of perturbations (denoted EG) and super-exponential growth of perturbations (denoted SEG).

or as perturbations to it grow. By considering how these boundaries move due to changes in $h$ or $Z$, the evolution of the mantle lithosphere's thermal structure can be examined. Consider mantle lithosphere for which $Z_0'=10$ per cent, $B_m=10^{10}$ Pa $s^{1/3}$, $h=25$ km and $t_{100}=50$ Myr. Initially, such a lithosphere grows most rapidly by cooling from above (Fig. 14a). However, as it thickens, $Ra_1$ increases, causing the transitional boundary of $P=1$ to move towards larger values of $t_{100}$. By the time the lithosphere is 50 km thick (Fig. 14b), such mantle lithosphere grows most rapidly by horizontal shortening. Alternatively, if the shortening rate increases due to an acceleration of convergence at the surface, $t_{100}$ should decrease, causing a transition from thermal diffusion to horizontal shortening as the most rapid mechanism (Fig. 14a).

The thickness of the mantle lithosphere should continue to increase, either by cooling from above or by horizontal shortening, until the lithospheric layer becomes convectively unstable. In fact, it can be argued that continental lithosphere is probably close to its stability limit for long portions of the Earth's history. The lithospheric roots beneath the cratonic shields, for example, are thought to have experienced little deformation since the Archaean (e.g. Hoffman 1990). Without any deformation, cooling from the surface since that time should cause the lithosphere to grow several times thicker than its maximum depth, which has been estimated at up to 200–300 km (e.g. Gaherty & Jordan 1995; Jaupart *et al.* 1998; Jordan 1988; Simons *et al.* 1999). Clearly, some erosion of the lithospheric base must occur to limit the lithospheric depth, even if the lithospheric root is partially stabilized due to an inherent chemical buoyancy, as has been proposed for the continental 'tectosphere' (e.g. Jordan 1978, 1981, 1988). If the erosion process involves convective instability, then the continental lithosphere should be at or near its stability limit, which is given by $Ra_1=100$ or $Ra_3=100$.

Consider mantle lithosphere that is tectonically stable (not shortening) and that has grown to its stability limit, for which $Ra_3=100$. The thickness of such lithosphere is given by the value of $h$ that produces $Ra_3=100$ for values of $Z_0'$ and $B_m$ appropriate for the lower lithosphere (Figs 14 and 15). For example, if $Z_0'=10$ per cent and the experimentally observed value of $B_m\sim10^{9.1}$ Pa $s^{1/3}$ applies, only mantle lithosphere thinner than $\sim$25 km is stable to convection (Fig. 14a). If mantle lithosphere thicker than this value can remain stable, $B_m$ must be greater or $Z_0'$ must be smaller. In fact, an order of magnitude increase in $B_m$ is required to increase the maximum thickness of stable lithosphere to 100 km (Fig. 14c). An increase in $B_m$ with lithosphere thickness is perhaps expected due to the pressure dependence of dislocation creep (e.g. Karato & Wu 1993). In addition, it is possible that uncertainties in estimates of $F_3$ or in the application of laboratory measurements of $B_m$ to the lithosphere could conspire to permit layers that are more than 100 km thick to be stable to small-scale convection at their bases.

If horizontal convergence is applied to a layer that is close to its stability limit ($Ra_3=100$), gravitational instability can be initiated rapidly. An increase in the background horizontal strain rate, $\dot{\varepsilon}_{xx}$, corresponds to a decrease in the time to 100 per cent thickening, given by $t_{100}$ in eq. (29). As shown in Figs 14 and 15, a sufficiently large decrease in $t_{100}$ along the $Ra_3=100$ curve causes exponential growth of perturbations to dominate deformation of the layer. For example, if $B_m\sim10^{10.1}$ Pa $s^{1/3}$ and $Z_0'=10$ per cent, mantle lithosphere of thickness $h=100$ km is stable to convection if shortening is sufficiently slow that $t_{100}>80$ Ma (Fig. 14c). For $t_{100}\sim30$ Myr, as seems to characterize Tibet (Molnar *et al.* 1993), the lithosphere is gravitationally unstable, with perturbations growing exponentially with time (Fig. 14c). Once perturbations begin to grow, the region for which $Ra_3>100$ (super-exponential growth of perturbations) begins to include larger values of $B_m$ (compare Figs 14 and 15). Thus, 100 km thick lithosphere for which $B_m=10^{10.1}$ Pa $s^{1/3}$ and $t_{100}=30$ Myr, but for which perturbations have increased to 50 per cent, should exhibit super-exponential growth of perturbations (Fig. 15c). In fact, if the layer is already at its stability limit before it begins thickening, super-exponential growth should begin after only a small increase in perturbation amplitude, meaning that the majority of the deformation should occur as super-exponential growth.

If the onset of horizontal convergence is not sufficient to initiate exponential growth, super-exponential growth may still develop after sufficient mechanical thickening. First, non-uniform horizontal shortening may increase the amplitude of perturbations, causing the layer to move from a state in which horizontal shortening dominates to one in which super-exponential growth dominates. If $B_m=10^{10.1}$ Pa $s^{1/3}$ and $h=100$ km, but $t_{100}$ decreases only to 100 Myr, an increase in

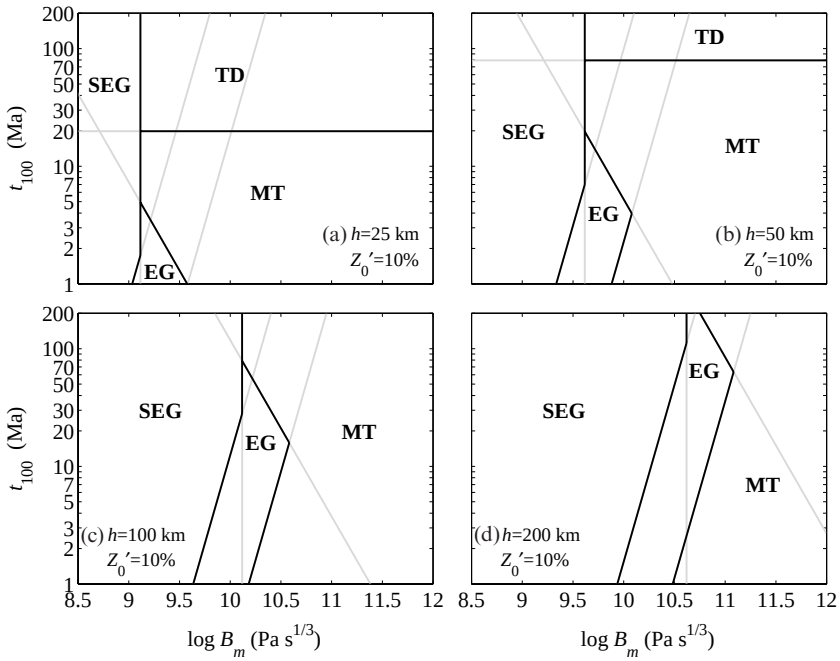


**Figure 14.** 'Phase diagrams' similar to the one exemplified in Fig. 13, but where the parameters relevant to the lithosphere (see text) are used to calculate the locations of boundaries between the different styles of thickening and growth. Shown in (a)–(d) are diagrams for mantle lithosphere with thicknesses of $h = 25$, 50, 100 and 200 km, and for an initial perturbation amplitude of $Z_0' = 10$ per cent.

perturbation amplitudes due to horizontal shortening should still cause super-exponential growth to become dominant (compare Figs 14c and 15c). Alternatively, an increase in layer thickness $h$ due to mechanical thickening should cause a marginally stable layer to become unstable (compare the location of $B_m = 10^{10.1}$ Pa $s^{1/3}$ and $t_{100} = 100$ Myr in Figs 14c and d).

Once super-exponential growth begins, the time for the initial gravitational instability to remove the bottom part of the mantle lithosphere can be estimated by making eq. (11) dimensional using eq. (9), which for $n = 3$ can be written as

$$t_b = \frac{h^2}{\kappa Ra_3} \frac{1}{2C^3} . \tag{31}$$

Because super-exponential growth begins when $Ra_3 = 100$, with $C = 0.45$ the removal time can be written as $t_b = 0.055h^2/\kappa$. With $\kappa = 10^{-6}$ $m^2$ $s^{-1}$, $t_b$ becomes a function of only the layer

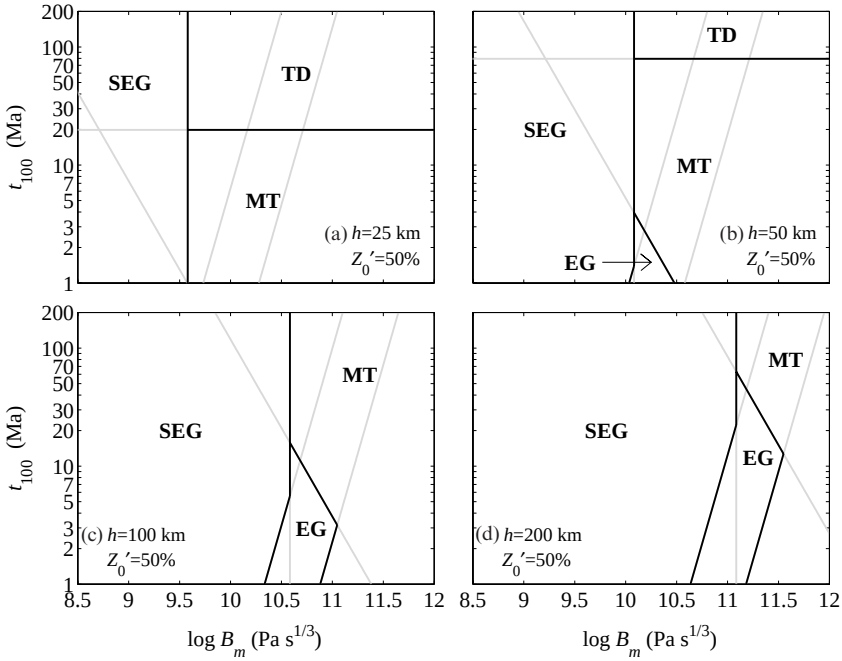


**Figure 15.** Similar to Fig. 14, but for a perturbation amplitude of $Z_0' = 50$ per cent. A comparison to Fig. 14 shows that the region in which super-exponential growth of perturbations dominates (denoted SEG) is larger for larger $Z_0'$.

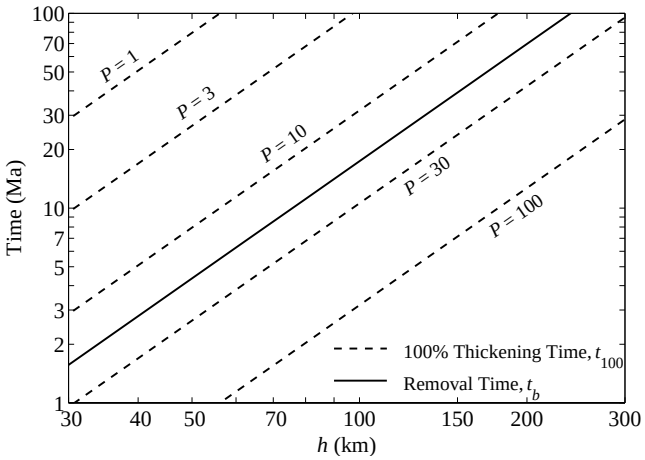


**Figure 16.** Plot of the time, $t_b$, for the initial instability to remove the base of the mantle lithosphere, and of the time, $t_{100}$, for 100 per cent thickening of the lithosphere (or 50 per cent shortening) to occur. Both $t_b$ and $t_{100}$ are calculated as described in the text as a function of the thickness, $h$, of the mantle lithosphere. The 100 per cent thickening time depends on the shortening rate, expressed here in terms of $P$.

thickness, $h$ (Fig. 16). All of the other parameters that affect growth are eliminated from this expression by the assumption that super-exponential growth begins when $Ra_3 = 100$. If, as discussed above, a phase of exponential growth or shortening precedes super-exponential growth, its duration should be short and thus should not significantly affect this estimate of $t_b$.

As discussed above, the amount of material removed by the initial instability depends primarily on the temperature dependence of viscosity. If, as is likely to be the case, viscosity varies by a factor of more than 100 across the mantle lithosphere, at most only the hottest 30 per cent of the mantle portion of the lithosphere can participate in downwelling and ultimately be removed (Fig. 10). If shortening continues after this time, however, the ongoing addition of cold material to the lithosphere is balanced by a persistent downwelling that removes this extra cold mantle lithosphere from the shortening region. If shortening is sufficiently fast and is allowed to occur indefinitely, this downwelling is capable of producing lateral temperature variations below the shortening region with amplitudes of up to 90 per cent of the total temperature variation across the cold layer (Figs 8 and 12).

The total amount of lithospheric shortening that occurs in the Earth may be limited to 50 per cent. As a result, the amount of time during which a persistent downwelling can develop may be limited as well. The time to 50 per cent shortening (100 per cent thickening) can be compared to the time for the initial instability to occur by taking the ratio of $t_{100}$ and $t_b$ using eqs (29) and (31). Simplifying using $Ra_3 = 100$ and $C = 0.45$ shows that $t_{100} = t_b/(0.055P)$. Thus, the time to 50 per cent shortening is some multiple of the initial removal time, where this multiple depends on $P$ (Fig. 16). If shortening is sufficiently fast that $P > 1/0.055 \sim 18$, mechanical thickening of the layer should occur more rapidly than convective instability, meaning that an estimate of $t_b$ is probably not relevant. As shown in Fig. 16, $P > 18$ requires 100 km thick mantle lithosphere to double in thickness in only 15 Myr, and thinner lithosphere to shorten even more rapidly. This is faster than the $\sim 30$ Myr expected for shortening by 50 per cent in Tibet (Molnar *et al.* 1993), but implies horizontal strain rates of $\sim 10^{-15}$ s$^{-1}$, which are perhaps not unreasonable for other convergent zones such as the Transverse Ranges of California (e.g. Houseman *et al.* 2000).

On the other hand, if shortening is slow enough that $P < 18$, then $t_{100} > t_b$, meaning that 50 per cent shortening occurs after the initial removal event. In this case, only the hottest 60 per cent of material is advected into the mantle (Fig. 12). Because the persistent downwelling removes material that is advected into the downwelling region, its amplitude depends on the amount of shortening that occurs. Thus, for shortening of 50 per cent, the amount of material that participates in the downwelling is a constant. This amount (the hottest $\sim 60$ per cent, corresponding to $\sim 500$ °C of temperature variation if the mantle lithosphere accounts for $\sim 800$ °C) is a larger fraction of the lithosphere than is observed to participate in the initial instability (at most the hottest $\sim 30$ per cent or $\sim 250$ °C), making the persistent downwelling a potentially more important consequence of shortening than the initial removal event.

A possible limitation of this analysis is that it is performed in only two dimensions, meaning that downwellings are necessarily sheet-like structures. This limitation is perhaps acceptable because this study is designed to treat instability that is generated by horizontal shortening, which, for convergence between two large plates, is inherently a 2-D process. Because, however, instabilities grow exponentially or super-exponentially with time, small lateral differences in growth rate can be rapidly amplified, causing a downwelling sheet to have a 3-D structure, which could complicate the application of these results to the mantle. In addition, these results treat dislocation creep, for which $n \sim 3$. Thus, regions of low strain rate resist flow because their effective viscosity is high. It is possible that flow in the asthenosphere is instead Newtonian, with a viscosity as low as $10^{19}$ Pa s (e.g. Hager 1991). In this case, the viscosity beneath the lithosphere would not be dictated by the background shortening rate, and thus would allow the lower lithosphere to be removed more rapidly, even at lower shortening rates than the above analysis suggests. On the other hand, deflection of the Moho is also ignored, which, if driven by convective instability, should tend to resist convective instability because it is gravitationally unfavourable (e.g. Houseman *et al.* 2000; Neil & Houseman 1999). Moho deflection may, however, also promote convective instability by generating large-amplitude perturbations to the mantle lithosphere's thermal structure.

## CONCLUSIONS

The theory and numerical experiments described above examine the deformation of unstable mantle lithosphere that is undergoing active shortening. The thermal structure of mantle lithosphere evolves due to four processes. In the absence of convective instability, mantle lithosphere thickens either by horizontal shortening or by cooling from above. Convective instability manifests itself either by the exponential growth of perturbations, which requires lithospheric viscosity to be set by the background shortening rate, or by the super-exponential growth of these perturbations, in which case viscosity is set by the strain rates associated with instability. The conditions under which each type of deformation is dominant can be determined by comparing the amplitudes of the dimensionless parameters $Ra_1$, $Ra_3$, $P$ and $Z_0'$, which are defined for this purpose (Table 1).

In applying these results, mantle lithosphere is assumed to have cooled sufficiently that $Ra_3 \sim 100$, meaning that it is nearly convectively unstable. In this case, horizontal shortening can easily initiate convective instability by increasing the amplitude of perturbations, either directly through non-uniform thickening, or by lowering the background viscosity so that perturbations begin to grow exponentially with time. Once super-exponential growth begins, the time for removal is approximately $t_b = 0.055h^2/\kappa$. Thus, for mantle lithosphere 100 km thick, the initial removal event occurs 17 Myr after shortening initiates super-exponential growth. For strongly temperature-dependent viscosity, at most only the hottest 30 per cent of the mantle lithosphere is involved in this event.

As shortening of the lithosphere continues, downwelling of lithospheric material persists after the initial removal event. This downwelling removes material that is continually being added to the layer by shortening, and thus is more substantial for larger shortening rates. Geological evidence suggests, however, that the total amount of shortening may be limited to 50 per cent, corresponding to thickening of 100 per cent (doubling of crustal thickness). Thus, shortening may cease before this downwelling can fully develop. Because this persistent downwelling removes material added to the lithosphere by shortening, its amplitude depends on the amount of shortening that occurs. For 50 per cent shortening, the hottest 60 per cent of the mantle lithosphere participates in the downwelling (Fig. 12). Thus, the downwelling that results from ongoing mechanical thickening of the layer is more substantial than the preceding downwelling associated with the initial removal event.

If mechanical thickening stops after achieving 50 per cent shortening, the downwelling that extends into the mantle beneath the shortening region is no longer replenished by the addition of lithosphere above it. As a result, this downwelling 'finger' is not likely to survive once horizontal shortening stops, but should instead be removed due to its own gravitational instability or by mantle shear. The replacement of this cold, downwelling fluid by hot, buoyant asthenosphere should cause significant uplift at the surface, a scenario related to the generation of uplift following the cessation of subduction and the subsequent removal of the descending slab (e.g. Mitrovica & Jarvis 1985). If uplift is generated in this way, it should immediately follow the cessation of shortening in a region. For Tibet, 50 per cent shortening (doubling of crustal thickness) began at 40–50 Ma and is thought to have taken 30–40 Myr to complete. Rapid uplift at the surface is inferred to have begun at approximately 8 Ma (Harrison *et al.* 1992; Molnar *et al.* 1993), after shortening had ceased within the interior of Tibet. This pattern is consistent with the gradual building of a cold protrusion into the mantle by horizontal shortening and rapid surface uplift associated with its removal once shortening stopped.

## ACKNOWLEDGMENTS

This work was supported in part by National Science Foundation grant EAR-9725648, and by a National Science Foundation Graduate Research Fellowship. I thank G. Houseman and an anonymous referee for constructive reviews, B. Hager for helpful comments and P. Molnar for suggestions and encouragement throughout the preparation of this manuscript that greatly improved its content and clarity.

## REFERENCES

Bassi, G. & Bonnin, J., 1988. Rheological modeling and deformation instability of lithosphere under extension, *Geophys. J. Int.,* **93,** 485–504.

Bird, P., 1979. Continental delamination and the Colorado Plateau, *J. geophys. Res.,* **84,** 7561–7571.

Canright, D. & Morris, S., 1993. Buoyant instability of a viscous film over a passive fluid, *J. Fluid Mech.,* **255,** 349–372.

Chandrasekhar, S., 1961. *Hydrodynamic and Hydromagnetic Stability,* Oxford University Press, Oxford.

Conrad, C.P. & Molnar, P., 1997. The growth of Rayleigh–Taylor-type instabilities in the lithosphere for various rheological and density structures, *Geophys. J. Int.,* **129,** 95–112.

Conrad, C.P. & Molnar, P., 1999. Convective instability of a boundary layer with temperature- and strain-rate-dependent viscosity in terms of 'available buoyancy', *Geophys. J. Int.,* **139,** 51–68.

England, P. & Houseman, G., 1986. Finite strain calculations of continental deformation 2. Comparison with the India–Asia collision zone, *J. geophys. Res.,* **91,** 3664–3676.

England, P. & Houseman, G., 1989. Extension during continental convergence, with application to the Tibetan plateau, *J. geophys. Res.,* **94,** 17 561–17 579.

England, P. & Searle, M., 1986. The Cretaceous-Tertiary deformation of the Lhasa block and its implications for crustal thickening in Tibet, *Tectonics,* **5,** 1–14.

Fleitout, L. & Froidevaux, C., 1982. Tectonics and topography for a lithosphere containing density heterogeneities, *Tectonics,* **1,** 21–56.

Fletcher, R.C. & Hallet, B., 1983. Unstable extension of the lithosphere: a mechanical model for Basin-and-Range structure, *J. geophys. Res.,* **88,** 7457–7466.

Gaherty, J.B. & Jordan, T.H., 1995. Lehmann discontinuity as the base of an anisotropic layer beneath continents, *Science,* **268,** 1468–1471.

Hager, B.H., 1991. Mantle viscosity: a comparison of models from postglacial rebound and from the geoid, plate driving forces and advected heat flux, in *Glacial Isostasy, Sea-Level and Mantle Rheology,* pp. 493–513, eds Sabadini, R., Lambeck, K. & Boschi, E., Kluwer, Dordrecht.

Harrison, T.M., Copeland, P., Kidd, W.S.F. & Yin, A., 1992. Raising Tibet, *Science,* **255,** 1663–1670.

Hirth, G. & Kohlstedt, D.L., 1996. Water in the oceanic upper mantle: implications for rheology, melt extraction and the evolution of the lithosphere, *Earth planet. Sci. Lett.,* **144,** 93–108.

Hoffman, P.F., 1990. Geological constraints on the origin of the mantle root beneath the Canadian shield, *Phil. Trans. R. Soc. Lond.,* **A331,** 523–532.

Houseman, G.A. & Molnar, P., 1997. Gravitational (Rayleigh–Taylor) instability of a layer with non-linear viscosity and convective thinning of continental lithosphere, *Geophys. J. Int.,* **128,** 125–150.

Houseman, G.A., McKenzie, D.P. & Molnar, P., 1981. Convective instability of a thickened boundary layer and its relevance for the thermal evolution of continental convergent belts, *J. geophys. Res.,* **86,** 6115–6132.

Houseman, G.A., Neil, E.A. & Kohler, M.D., 2000. Lithospheric instability beneath the Transverse Ranges of California, *J. geophys. Res.,* in press.

Howard, L.N., 1964. Convection at high Rayleigh number, in *Proc. 11th Int. Congress of Applied Mechanics,* pp. 1109–1115, ed. Görtler, H., Springer, New York.

Jaupart, C., Mareschal, J.C., Guillou-Frottier, L. & Davaille, A., 1998. Heat flow and thickness of the lithosphere in the Canadian Shield, *J. geophys. Res.,* **103,** 15 269–15 286.

Jordan, T.H., 1978. Composition and development of the continental tectosphere, *Nature,* **274,** 544–548.

Jordan, T.H., 1981. Continents as a chemical boundary layer, *Phil. Trans. R. Soc. Lond.,* **A301,** 359–373.

Jordan, T.H., 1988. Structure and formation of the continental tectosphere, in *J. Petrology,* Special Vol., pp. 11–37, eds Menzies, M.A. & Cox, K.G., Oxford University Press, Oxford.

Karato, S.-I. & Wu, P., 1993. Rheology of the upper mantle: a synthesis, *Science,* **260,** 771–778.

Karato, S.-I., Paterson, M.S. & FitzGerald, J.D., 1986. Rheology of synthetic olivine aggregates: influence of grain size and water, *J. geophys. Res.,* **91,** 8151–8176.

King, S.D., Raefsky, A. & Hager, B.H., 1990. ConMan: vectorizing a finite element code for incompressible two-dimensional convection in the Earth's mantle, *Phys. Earth planet. Inter.,* **59,** 195–207.

Kohlstedt, D.L., Evans, B. & Mackwell, S.J., 1995. Strength of the lithosphere: constraints imposed by laboratory experiments, *J. geophys. Res.,* **100,** 17 587–17 602.

Le Pichon, X., Fournier, M. & Jolivet, L., 1992. Kinematics, topography, shortening, and extrusion in the India-Eurasia collision, *Tectonics,* **11,** 1085–1098.

Mitrovica, J.X. & Jarvis, G.T., 1985. Surface deflections due to transient subduction in a convecting mantle, *Tectonophysics,* **120,** 211–237.

Molnar, P. & Tapponnier, P., 1978. Active tectonics of Tibet, *J. geophys. Res.,* **83,** 5361–5375.

Molnar, P., England, P. & Martinod, J., 1993. Mantle dynamics, uplift of the Tibetan plateau and the Indian monsoon, *Rev. Geophys.,* **31,** 357–396.

Molnar, P., Houseman, G.A. & Conrad, C.P., 1998. Rayleigh–Taylor instability and convective thinning of mechanically thickened lithosphere: effects of non-linear viscosity decreasing exponentially with depth and of horizontal shortening of the layer, *Geophys. J. Int.,* **133,** 568–584.

Neil, E.A. & Houseman, G.A., 1999. Rayleigh–Taylor instability of the upper mantle and its role in intraplate orogeny, *Geophys. J. Int.,* **138,** 89–107.

Platt, J.P. & England, P.C., 1994. Convective removal of lithosphere beneath mountain belts: thermal and mechanical consequences, *Am. J. Sci.,* **294,** 307–336.

Platt, J.P., Soto, J.-I., Whitehouse, M.J., Hurford, A.J. & Kelley, S.P., 1998. Thermal evolution, rate of exhumation, and tectonic significance of metamorphic rocks from the floor of the Alboran extensional basin, western Mediterranean, *Tectonics,* **17,** 671–689.

Rayleigh, Lord (Strutt, J.W.), 1916. On convection currents in a horizontal layer of fluid, when the higher temperature is on the under side, *Phil. Mag.,* **32,** 529–546.

Ricard, Y. & Froidevaux, C., 1986. Stretching instabilities and lithospheric boudinage, *J. geophys. Res.,* **91,** 8314–8324.

Simons, F.J., Zielhuis, A. & van der Hilst, R.D., 1999. The deep structure of the Australian continent inferred from surface wave tomography, *Lithos,* **48,** 17–43.

Turcotte, D.L. & Schubert, G., 1982. *Geodynamics,* John Wiley, New York.

Whitehead, J.A. & Luther, D.S., 1975. Dynamics of laboratory diapir and plume models, *J. geophys. Res.,* **80,** 705–717.

Zuber, M., Parmentier, E.M. & Fletcher, R.C., 1986. Extension of continental lithosphere: a model for two scales of Basin and Range deformation, *J. geophys. Res.,* **91,** 4826–4838.